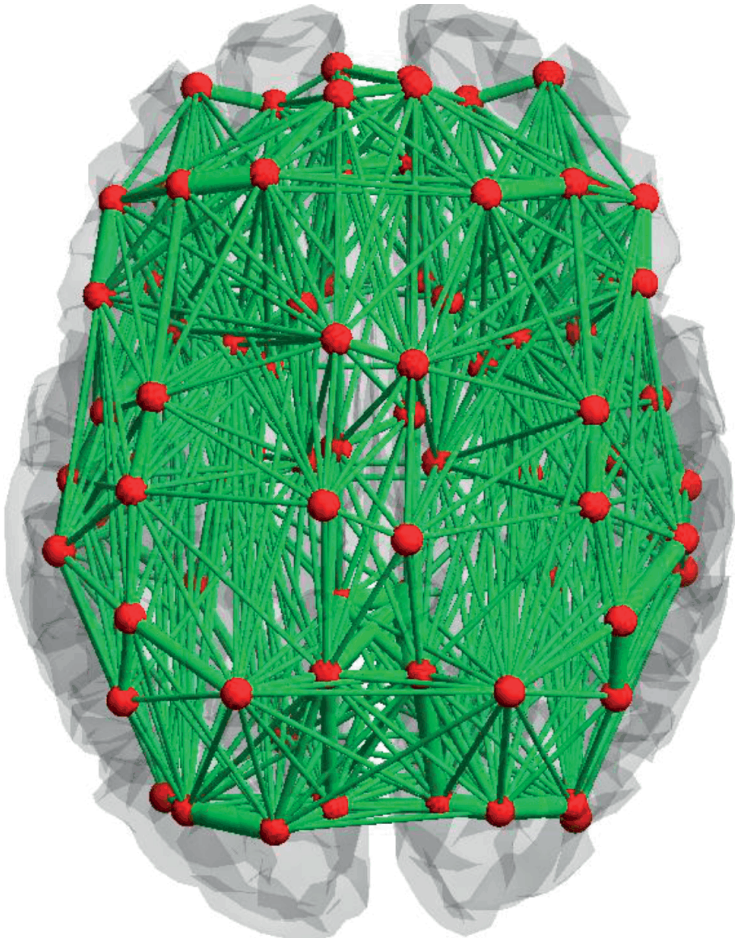

António Angelo Gouveia Rosa Perez de Almeida

ROLE OF INTERHEMISPHERICAL CONNECTIONS IN RESTING-STATE FUNCTIONAL CONNECTIVITY

Dissertação de Mestrado na área cientifica de Engenharia Biomédica, especialidade de Neurociências, orientada pela Professora Doutora Maria José Braga Marques Ribeiro e apresentada ao Departamento de Física da Faculdade de Ciência e Tecnologia da Universidade de Coimbra.

Coimbra, 2015

· U C ·

Universidade de Coimbra

• U C •

FCTUC FACULDADE DE CIÊNCIAS
E TECNOLOGIA
UNIVERSIDADE DE COIMBRA

António Angelo Gouveia Rosa Perez de Almeida

Role of interhemispherical connections in resting-state Functional Connectivity

Dissertação apresentada à Universidade de Coimbra para cumprimento dos requisitos necessários à obtenção do grau de Mestre em Engenharia Biomédica

Orientador(es):
Maria Ribeiro (Institute for Biomedical Imaging and Life Sciences)
Joana Cabral (University of Oxford)

Coimbra, 2015

Este trabalho foi desenvolvido em colaboração com:

Universidade de Coimbra

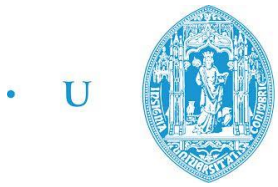

FCTUC FACULDADE DE CIÊNCIAS E TECNOLOGIA UNIVERSIDADE DE COIMBRA

Institute for Biomedical Imaging and Life Sciences

iBiLi Institute for Biomedical Imaging and Life Sciences University of Coimbra

University of Oxford

UNIVERSITY OF OXFORD

Declaration of Authorship

"*I'm reaching for the random or whatever will bewilder me.*
Following our will and wind we may just go where no one's been.
We'll ride the spiral to the end and may just go where no one's been.
Spiral out. Keep going."

—Tool, *in* Lateralus

UNIVERSITY OF COIMBRA

Abstract

Faculty of Sciences and Technology

Masters Degree in Biomedical Engineering

by António Angelo Gouveia Rosa Perez de Almeida

The purpose of this thesis was to identify the role of interhemispherical connections in resting-state functional connectivity. Studying brain function in resting-state gives insight into patterns in anatomical connectivity and is increasingly important both as a proxy measure for structural connectivity and as a biomarker for brain changes in disease. We used the Kuramoto Model of Time Delays and Coupled Oscillators to evaluate the effect of reducing the strength of interhemispheric connections on the functional network of the brain, both with and without preserving the Anterior Commissure. Our findings indicate a monotonic reduction in interhemispheric functional connectivity as the strength of structural connections diminish, an increase of intrahemispheric connectivity as the strength of structural connections diminish below 40% of their original value and a unmistakable preservation of functional connectivity after total interhemispheric section when the anterior commissure is preserved, albeit with important quantitative changes in the network. These results present one more step in the way towards complete understanding of human brain.

UNIVERSITY OF COIMBRA

Resumo

Faculty of Sciences and Technology

Masters Degree in Biomedical Engineering

por António Angelo Gouveia Rosa Perez de Almeida

O objectivo desta tese foi a identificação do impacto das ligações inter-hemisféricas na conectividade funcional em estado de repouso. O estudo da função cerebral em estado de repouso permite a compreensão de padrões na conectividade anatómica e é cada vez mais importante, quer como uma medida indirecta da conectividade estrutural e como um biomarcador de alterações cerebrais em doena. Neste trabalho usamos o modelo de Kuramoto com atrasos temporais e osciladores acoplados para avaliar o efeito de reduzir a força de ligações inter-hemisféricas na rede funcional do cérebro, com preservação e secção da comissura anterior. Os nossos resultados indicam uma redução monotónica na conectividade funcional inter-hemisférica à medida que a força das ligações estruturais diminui, um aumento na conectividade intra-hemisférica quando a força as ligações estruturais diminui abaixo de 40% do seu valor original e preservação da conectividade funcional após secção total das ligações inter-hemisféricas quando a comissura anterior é preservada, apesar de que, com elevadas mudanças qualitativas na rede. Estes resultados são mais um passo no caminho para a total compreensão do cérebro humano.

Acknowledgements

First of all, I would like to express my most sincere gratitude to Professor Maria Ribeiro for her valuable and constructive suggestions, patient guidance and her willingness to give her time so generously.

My grateful thanks are also extended to Professor Joana Cabral for her enthusiastic encouragement and precious support in this research work.

A very special *thank you* to my loving and supporting family, for the patience and incentive they have always shown. I owe them everything and this work is no exception.

I would also like to all the friends I am blessed to have. You have always stood beside me through thick and thin and for that I can't thank you enough. You guys are awesome.

Last but not least I would like to thank my girlfriend. With you by my side the future doesn't seem so daunting after all.

Contents

List of Figures

List of Tables

Abbreviations

AC	**A**nterior **C**ommissure
AgCC	**C**allosal **A**genesis
CC	**C**orpus **C**allosum
FC	**F**unctional **C**onnectivity
SC	**S**tructural **C**onnectivity

To my Parents;

So intrinsic to me,
I am occasionally them.

Chapter 1

Introduction

Studying brain function during rest in the absence of task demands has proven to be a valuable tool for characterization of spontaneous brain functional structure.This is refered to as resting-state functional connectivity and reveals interactions between various brain regions showing correlations in spontaneous brain activity in the absence of external stimuli or task demands. This reflects patterns in anatomical connectivity and is increasingly important both as a proxy measure for structural connectivity and as a biomarker for brain changes in disease. However, to understand the relationship between changes in functional connectivity and physiological changes in the brain tissue we need to investigate how the physical integrity of the brain influences the correlations in functional connectivity. In this work, we evaluate the effect of reducing the strength of interhemispheric connections on the functional network of the brain, both with and without preserving the anterior commissure. With this we hope to shed light on the role of interhemispherical connections in resting-state functional connectivity.

1.1 Motivation And Goals

A complete understanding of the human brain is one of the greatest challenges facing modern science. We have reached a point where we know more about the human brain than ever before but still not enough by far. Recent advances in imaging technology have brought us answers, but multiple questions as well, as is often the case in science. This has led to an unprecedented international

push towards fully comprehending this most complex of organs in what could be described as our generations race to the moon.

However if we truly wish to achieve this goal a method of simplifying the overwhelming complexity of brain dynamics must be used. A possible approach would be to model the human brain, using abstraction to reduce the cortical network to a tractable approximation capable of providing further insight into the laws governing the cerebrum. Indeed, such models have already been used to successfully reproduce features of macroscopic cortical dynamics. With this in mind, we used the Kuramoto Model of Phase Oscillators and Time Delays [1] in order to generate interpretable data from neural simulations.

In this work, we set out with the objective of providing further insight into the role that structural connections between hemispheres play in normal brain function. Dysfunction in these interhemispherical connections are related to multiple pathologies further incentivizing research in this subject. To this end, we simulated various states of structural damage, from intact to complete section of these interhemispheric connections.

1.2 Thesis Structure

This thesis is divided into 6 distinct chapters, where each chapter is divided into sections and sub-sections. This chapter provides a general introduction of this work. It is followed by a brief overview of the theoretical concepts needed to understand our research, as well a description of relevant previous studies. In the third chapter we introduce the methodology that was followed in this work. In the fourth we present the results we obtained and discuss them in chapter five. The final chapter concludes this work with a review of our results, conclusions as well as sugestions for future work.

Chapter 2

Theoretical Background

In this chapter we review the theoretical basis of this work. We begin with an illustration of the brains networks, both relative to structure and function, its activity during rest and all necessary introductory concepts to fully understand the thesis. This is then followed by an overview of the best understood interhemispheric connections, the Corpus Callosum and the Anterior Commissure, describing their anatomy and the most common pathologies they are affected by. This chapter ends with a detailed description of the model used to simulate the human brain. The importance of models like this cannot be understated, as with such tools we have a means of exploring neural processes in ways that are simply not possible *in vivo* and with virtually no monetary cost.

2.1 Structural and Functional Connectivity

The understanding of the human brain has been a long-lasting goal for the scientific community ever since the first anatomical studies were performed. Anatomical studies of ever-increasing complexity have allowed for a remarkable wealth of knowledge on the brain's structural organization. We now recognize the brain as a complex network of distinct brain areas with specialized functions communicating through axonal fibers.

Despite this, our understanding of the mechanisms leading to its function has lagged behind. This is so because the brain is responsible for a variety of tasks despite a fixed anatomy, a characteristic that distinguishes it from the remaining

organs which present a 1:1 ratio of anatomy to function. Sporns [2] suggests that valuable insight into this problem may be gathered by furthering our understanding on the organization of the neuro-anatomical network. Indeed, recent studies indicate that the coordination required for functional integration may arise from the brain's network architecture [3] [4].

This brought to light the need to understand the relationship between structural networks (connectivity), the physical connections between neural regions, and functional connectivity, the patterns of dynamic interactions [5]. Research shows that the underlying structural connectivity influences resting-state functional connectivity [6] [7]. Resting-state describes a wakeful brain in the absence of tasks and will be further described in the Functional Connectivity subsection. However, while a physical link between two regions predicts functional connectivity, functional connectivity has been found to exist without direct structural connection [8] which suggests these to be mediated by indirect anatomical connections. A study by Hae-Jeong Park and Karl Friston [9] underlines the need for computational models of neural network dynamics to investigate these relationships. In this work we have used one such model to infer the alterations in resting-state functional connectivity caused by various degrees of loss in interhemispherical connectivity.

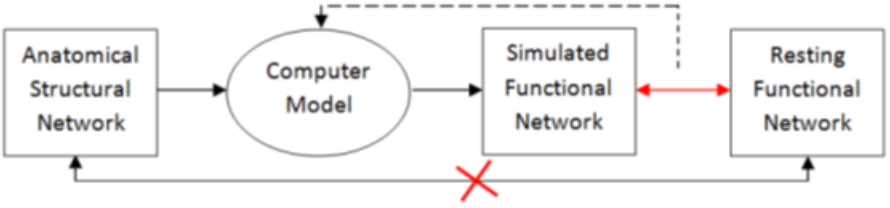

FIGURE 2.1: Diagram illustrating how computational models can serve to explore the relationship between anatomical structural networks and resting functional networks. The red line indicates comparison and the dashed line implies the need for feedback of the model's performance in order to fine-tune its parameters. The red cross simbolizes the lack of a direct comparison between structural and functional connectivity. Adapted from Cabral et al. [10]

.

In the following subsections, we will further describe structural and functional connectivity and how these networks are constructed.

2.1.1 Structural Networks

In order to accurately simulate the human brain its structural connectivity network must be mapped [12] [13]. This map of the brain's anatomical connectivity is known as the connectome. To map the cerebral cortex, a complex network believed

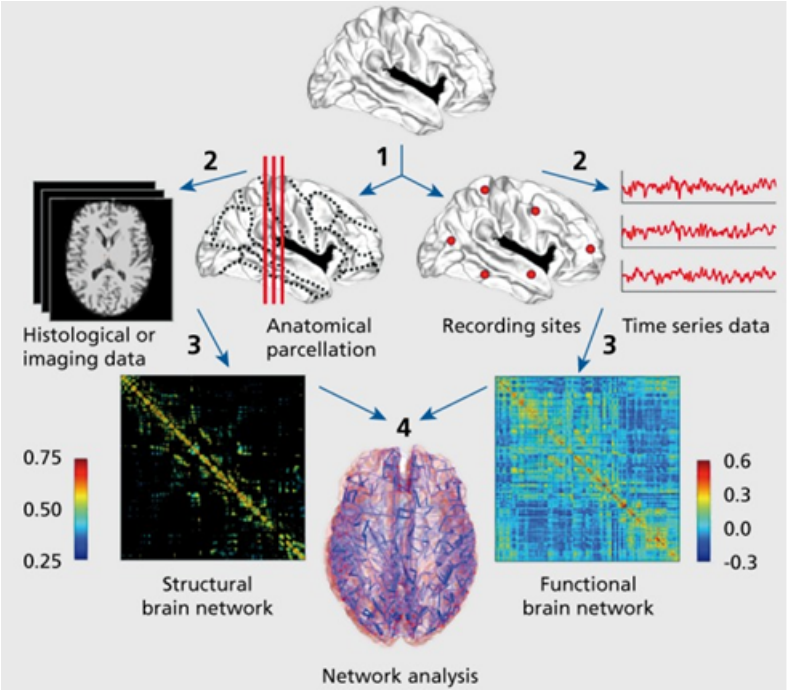

FIGURE 2.2: Basic workflow for extracting brain networks from neurological data. Adapted from Sporns [11].

to contain at least 10^{10} neurons, would be a herculean task but by focusing on the large-scale connections between cortical regions a map of the structural network becomes viable. This network would then contain a "blueprint" of the brain's organization, the major connections between neural regions that are the basis for communication in the brain.

Such a map of the brain's structural connectivity is only possible due to advances in noninvasive neuroimaging, with such a major leap forward that sparked the Human Connectome Project (www.humanconnectomeproject.org) and the Human Brain Project (www.humanbrainproject.eu) two international initiatives dedicated to establishing the largest possible library of neural information. Two techniques are the basis for creating the connectome, brain parcellation, and Diffusion Tensor Imaging (DTI) [14], as represented in fig. 2.2 ((1) and (2,left)).

The first step is to divide gray matter using brain parcellation, which is done according to a plan with the guidelines for determining partition between areas, the parcellation scheme. There are multiple versions of such templates described in literature [15], with various partition strategies, from traditional separation into lobes to division into several thousand regions of interest. Once a suitable parcellation scheme is selected, the number of fiber tracts, detected by DTI and

tractography, connecting regions are counted by computational algorithms, thus creating a connection matrix between the regions of interest (fig.2.3).

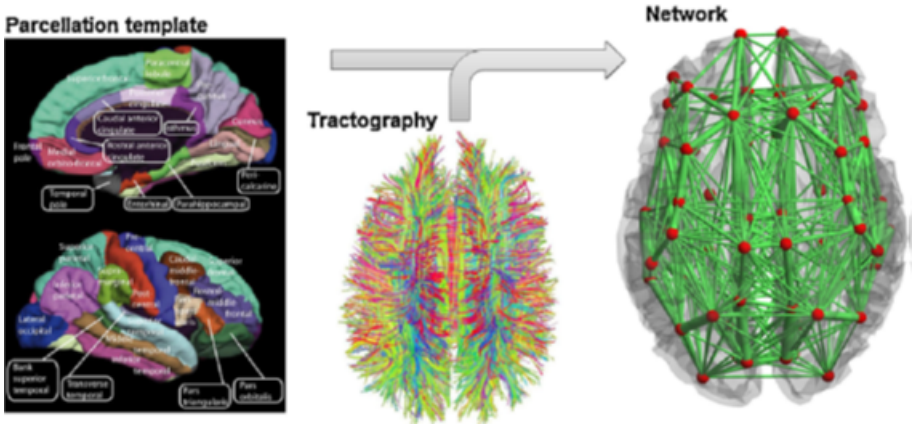

FIGURE 2.3: Building a 3-D structural network from the brains anatomical coupling architecture. Adapted from Cabral et al. [10].

DTI is a diffusion MRI method, a procedure that measures diffusion of water molecules in the brain. In an unrestricted environment water diffuses equally in all directions (isotropic diffusion). However, the brain presents a restricted environment where barriers, such as cell membranes, cause water to diffuse more readily in the direction of axons than perpendicular to their membrane. This uneven diffusion (anisotropic diffusion) allows DTI to infer the orientation of white matter tracts in the brain by measuring the strength and direction of the diffusion in each voxel. Then the fiber tracts are detected by estimating their trajectories using tractography.

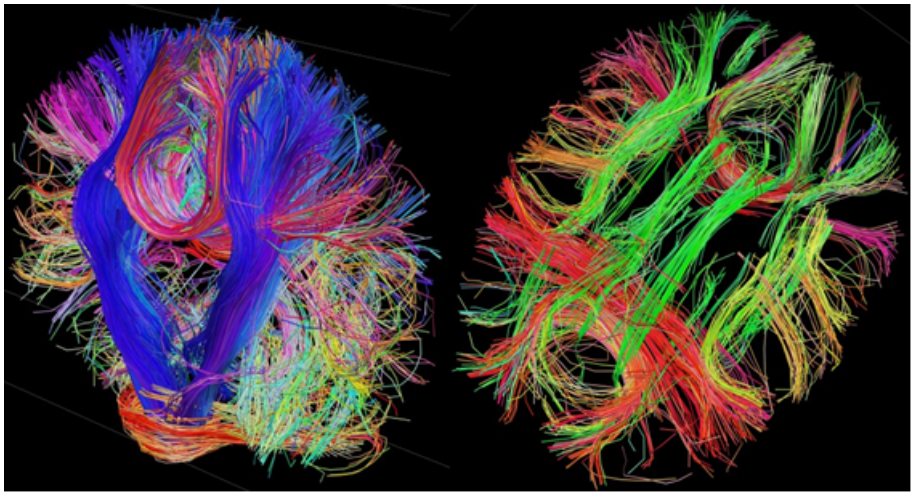

FIGURE 2.4: White matter fibres detected in vivo using Diffusion MRI. Images adapted from the gallery of the Connectome Project (www.humanconnectomeproject.org)

The resulting brain connectivity data can be represented in matrices, the Structural Connectivity matrix,C_{np}, (fig. 2.2, (3,left)) and the length matrix, L_{np}. For a

network with N cortical regions the matrices present N columns and N rows, where each entry corresponds to either the weight of connectivity C_{np}, proportional to the number of fibers detected, or the distance L_{np} between region n and region p. These matrices are further described in Modeling the Human Brain.

2.1.2 Functional Networks

As previously mentioned, functional connectivity reflects patterns of dynamic interactions between cortical regions [11] [5]. These dynamic interactions are represented in the statistical dependence of the activity of those regions and provide an indicator of cognitive function. In contrast to structural connectivity which is generally stable, functional networks are time-dependent, where the rapid reconfigurations are an indicator of a temporary brain state in which two separate areas share the same dynamic [3].

Functional networks are commonly derived from time-series data which can be obtained using multiple techniques such as electroencephalography (EEG), magnetoencephalography (MEG) and functional magnetic resonance imaging (fMRI) (fig. 2.2, (2,right)). Functional MRI in particular merits further discussion as it was the method through which the data used in this study was obtained. This technique has an indentical procedure to MRI, where, while MRI relies on the water molecules hydrogen nuclei, for fMRI the basic measure is the change in magnetization between high and low oxygen concentration in the blood. It does so by measuring the income of oxygen-rich blood to a determined cortical region, improving the magnetization of that region due to a reduction on the concentration of the paramagnetic deoxygenated haemoglobin (dHb) [16]. Because of this fMRI provides an indirect assessment on the activation of neural areas as it is the increase in oxygen-rich blood that is measured and not the real activation [17]. The changes in magnetization are detected across the brain by using the blood-oxygen-level-dependent contrast (BOLD) which is an acquisition method that increases the effect of dHb developed by Ogawa et al. [18]. Because dHb is a naturally present contrasting agent there is no need for invasive procedures to prepare for fMRI. There are two commonly used variations on fMRI, task-fMRI (T-fMRI) where a specific task is performed by the subjects and resting-state fMRI (R-fMRI) where the subject is awake, resting (fig. 2.5) [7].

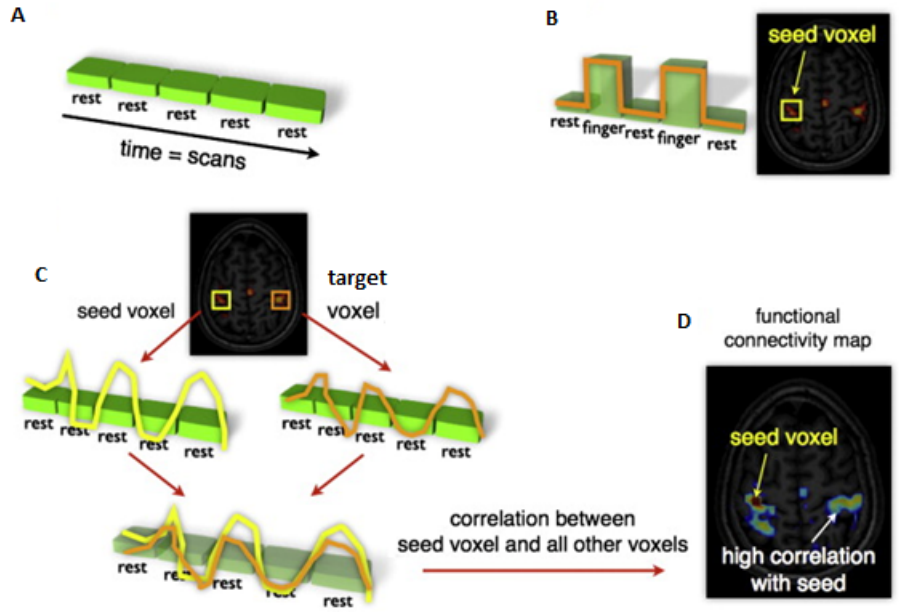

FIGURE 2.5: Schematic of the workflow of a resting-state fMRI study. (A) BOLD fMRI signal of a resting and awake subject is measured throughout the study. (B) The seed region of interest is chosen, possibly through conventional T-fMRI. (C) To determine functional connectivity between two regions the seed voxel is correlated with the target voxel. (D) The functional connectivity map is created by correlating the seed voxel with all other voxels in the brain, displaying all the regions that display high functional connectivity (high correlation) with the seed region. Adapted from Heuvel and Hulshoff [7].

Task-fMRI studies are typically used in activation studies, obtaining activation maps of average engagement of different cortical regions during the study by comparing the changes in neural activity induced by the test task, by the control task and the baseline, or resting-state (fig 2.6)[19]. However, both task and resting-state fMRI data can be used for studying functional connectivity, revealing the organization of several neural regions into large-scale networks, both in the presence, and absence, of a task response [20].

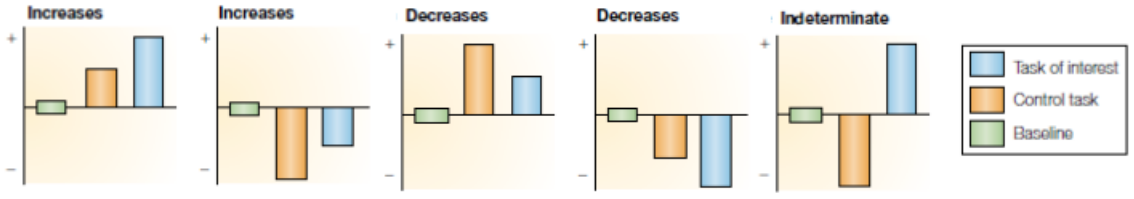

FIGURE 2.6: Scheme of how increases and decreases in activation are interpreted from T-fMRI data. Adapted from Gusnard and Raichle [19].

Regarding functional connectivity studies, T-fMRI and R-fMRI serve two distinct purposes. T-fMRI is used to study the functional connectivity from a source (or seed) region to another target region, as those regions are responsible for the brain function linked to the specific task demands, whereas R-fMRI focuses on functional communication networks within the brain during rest (resting-state). The most

common method to evaluate functional connectivity from resting-state is to determine the Pearson correlation between BOLD signals of two distinct regions. With this method a high correlation coefficient represents functional connection which occurs if the activation and deactivation of those regions is synchronized. With this correlation data the functional connectivity matrix is then constructed where each line displays the correlation of the BOLD signal between a individual region and all the remaining regions. This matrix has the same size as the structural matrix, where for a network with N cortical regions the matrix presents N columns and N rows (fig.2.2, (3, right)).

With this we need to further review what resting-state is, as the data used in this work is resting-state functional connectivity. An individual is considered to be at rest when no specific physical or mental tasks are performed while in a wakeful state. Despite being at rest, in this state the brain remains active, with clear organized neural activations, also known as resting-state functional connectivity. This was first proved in a study by Biswall et al. [21], where they presented high correlation between the BOLD signals of the primary motor network regions of both hemispheres during rest. Since then multiple studies have replicated and expanded upon these results, recognizing that the brain is not idle in this state, but rather shows spontaneous networks of highly correlated brain regions. Some of these correlations fluctuate in time and are present in wakeful rest, vanishing as a task is triggered or as the person falls asleep [22].

The idea that these networks are neural based and not artifacts or manifestations of other patterns produced by cardiac or respiratory cycles is supported by a high consistency of the results across multiple imaging methods, by the fact that the resting-state functional networks detected usually overlap with known functional networks detected during task related neural activity and the domination of lower frequencies ($<$0.1 Hz) in BOLD signals which are independent from heartbeat and respiratory frequencies [7].

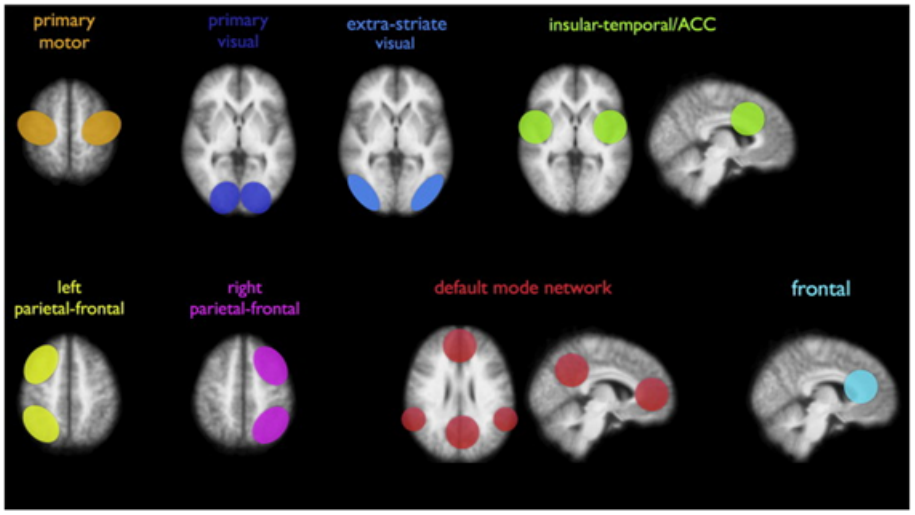

FIGURE 2.7: Resting state networks that are consistently found across multiple studies with different subject groups. Adapted from Heuvel and Hulshoff [7].

In the next section, we provide a description of interhemispherical connections, namely the best understood interhemispheric fiber tracts, the Corpus Callosum and the Anterior Commissure, and contextualize some of the relevant research on this topic that has been done to date.

2.2 Overview of the Interhemispheric Connections

Interhemispherical connections are constituted by multiple fiber bundles, the most prominent and best understood of which are the Corpus Callosum and the Anterior Commissure. The Anterior Commissure connects both hemispheres, crossing through the lamina terminalis, and is located in the anterior portion of the columns of the fornix [23]. Most nerve fibers connecting the hemispheres cross via the Corpus Callosum, but a small number alternatively pass through this fiber bundle, connecting the olfactory bulbs, olfactory nuclei, and the middle and inferior temporal gyri [15]. Thus, the pursuit for a greater understanding on the importance of interhemispheric connections would be fruitless without detailed and comprehensive knowledge about the structure containing the great majority of fibers connecting the left and right hemispheres, the Corpus Callosum (CC). It is by far the largest white matter tract in the human brain, consisting of approximately 190 million axons [24] and although at one point believed to serve no purpose other

than to keep both hemispheres from toppling onto each other [25], its importance has long since been recognized and is now believed to play an important role in cognition and is object of extensive research [26].

Located in the center of the human brain between hemispheres, the CC is topographically organized, that is to say arranged in such a way that groups of adjacent fibers connect a particular cortical area [27]. In order to provide anatomical description it is generally organized in four broad regions: genu or anterior bulbar end, the splenium or posterior rounded end, the isthmus or the area anterior to the splenium, and the body or the area between the genu and isthmus, as seen in fig.2.8. Regarding the white matter fibers that constitute each of these areas the genu and the anterior splenium are composed of high-density thin fibers, with low myelination and slow conduction, whereas, in the posterior splenium, exist large, highly myelinated and fast-conducting fibers [28]. The body is made of fast-conducting medium sized fibers that grow larger and more myelinated from the anterior end up to the posterior end, whereas the isthmus has a fiber organization that contradicts this pattern, being composed of smaller fibers than the ones in the posterior end of the body [28].

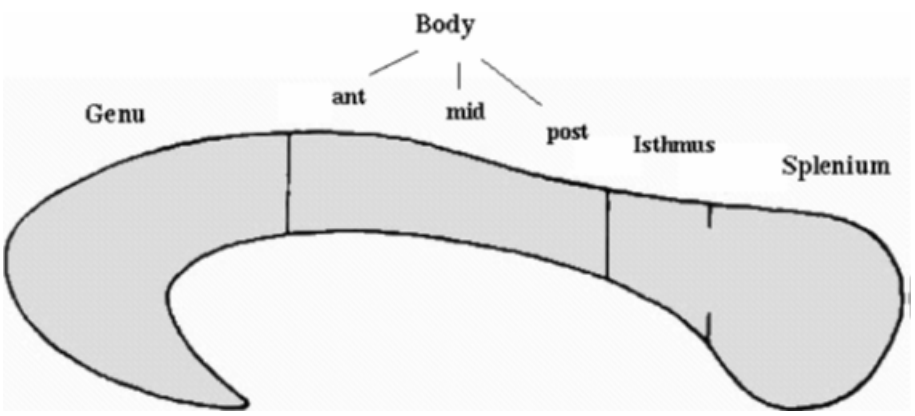

FIGURE 2.8: Schematic view of corpus callosum with the different subregions of the CC for nomenclature. Adapted from Aboitiz et al. [28].

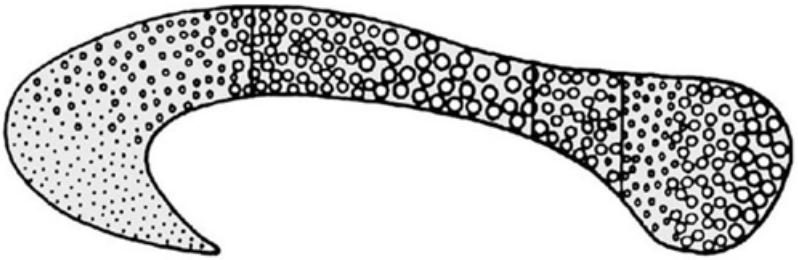

FIGURE 2.9: Scheme of a cross-section of the human corpus callosum illustrating the spatial distribution of fibers according to their diameter. Adapted from Aboitiz et al. [28].

Each of these areas associate specific regions, the genu connects the prefrontal association areas and the anterior inferior parietal regions [29] [30], the body connects premotor, supplementary and primary motor areas, and the isthmus connects primary motor as well as primary sensory areas [29] [31]. Lastly the anterior end of the splenium connects association areas of the parietal and temporal lobes and the posterior end links the occipital lobes.

Despite possessing both homotopic connectivity (connectivity from a region to its contralateral homolog) and heterotopic connectivity, the majority of fibers in the Corpus Callosum connect homotopic areas. In previous work, Stark et al. [32] studied the distribution of the correlation between such connections across the human brain using resting-state fMRI data from 62 healthy individuals. In their work they report correlation between homotopic connections to be significantly higher than nonhomotopic ones (intra and interhemispheric connections) [32]. With their study, Stark et al. [32] also found interhemispheric correlation to vary from region to region, with the highest correlation among homotopic connections to be for the primary sensory and motor cortices. The distribution of the average homotopic correlation is presented in fig. 2.10.

The Corpus Callosum, like any structure in the human body is subject to multiple pathologies that alter or impair its function. These can have multiple origins, ranging from myelination disorders, both hereditary (Krabbe's disease) and inflammatory (Multiple sclerosis), to trauma (Diffuse Axonal Injury) and to rare toxic pathologies (Marchiafava−Bignami) [33] [34].

Out of all pathologies however, callosal malformations are by far the most relevant to the understanding of this fiber tract. Callosal agenesis in particular provides a unique window to comprehend the CC. In the next section we will describe these congenital pathologies and their impact on brain function.

2.2.1 Congenital Pathologies of the Corpus Callosum

Normal development of the human CC begins after 10-13 weeks post conception and the development is completed within the first 4 years of life. However this is not infallible, with many problems liable to occur during this period, resulting in callosal malformations. These pathologies are referred to as congenital and include

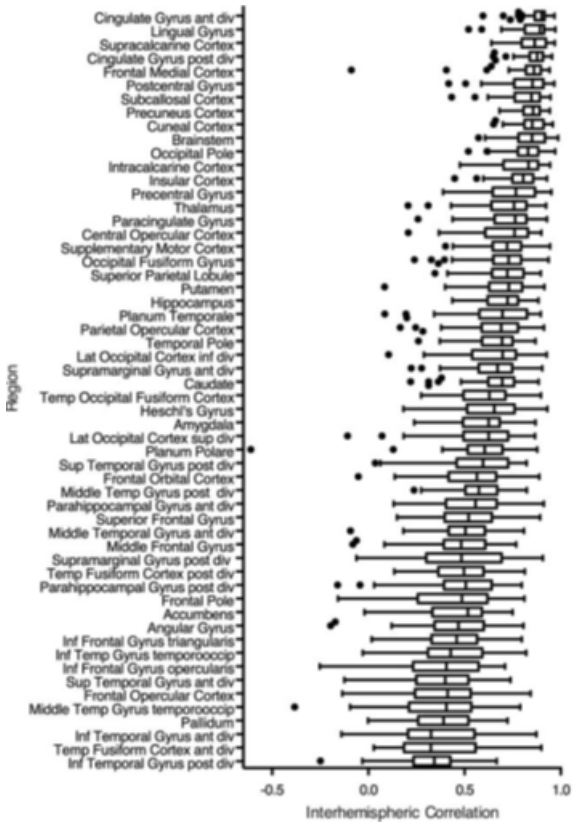

FIGURE 2.10: Tukey box-and-whiskers plots showing the distribution of interhemispheric correlations for all 56 homotopic regions across subjects (vertical line, median; box, interquartile range; whiskers, 1.5 times the interquartile range; closed circles, individual values lying outside 1.5 times the interquartile range). Adapted from Stark et al. [32].

agenesis (partial or complete absence of the CC), dysgenesis (malformation of CC), and hypoplasia (abnormality in CC).

As it is impossible to know how many of these remain undiagnosed, the incidence of such pathologies is hard to estimate but recent studies suggest a prevalence of 3-7 per 1000 births [33].

Out of the congenital pathologies the most studied remains the agenesis of the CC (AgCC). This malformation presents an exceptional opportunity to further our understanding of the CC, as its absence should shed light on CC functionality in an analogous manner to the knockout gene model. However a paradox soon surfaced, discovered by Roger Sperry, Nobel Prize winner in 1981. While patients with AgCC presented preserved interhemispheric communications, split brain subjects (subjects who underwent surgical transection of the corpus callosum) had no such capability, in fact, developing the disconnection syndrome, a condition caused by absence of information transfer between hemispheres. While this paradox is not yet fully understood a recent study shows that brain rewiring via anomalous fiber

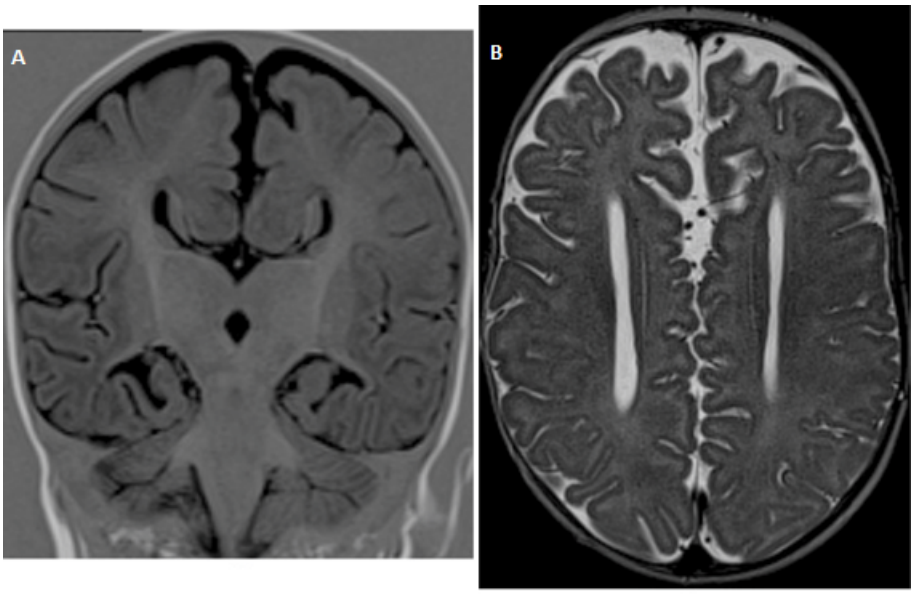

FIGURE 2.11: MR coronal image (a) and MR axial image (b) fluid-attenuated inversion recovery images show complete agenesis of the corpus callosum. Adapted from Fitsiori et al. [33].

tracts connecting both hemispheres explains the preservation of interhemispheric integration in AgCC [35].

These expectations are supported by the work of Owen et al. [36] where DTI studies indicate a rearrangement of interhemispheric connections in AgCC individuals. They also show higher variability in the structural connectome of AgCC subjects than controls. Further work by Owen et al. [36] expands on the effects of AgCC on functional networks. They found that while qualitatively these networks presented almost no variation from the controls (fig. 2.12) quantitative measures found greatly reduced functional connectivity in some intra-hemispheric and interhemispheric networks in subjects with AgCC (fig. 2.13).

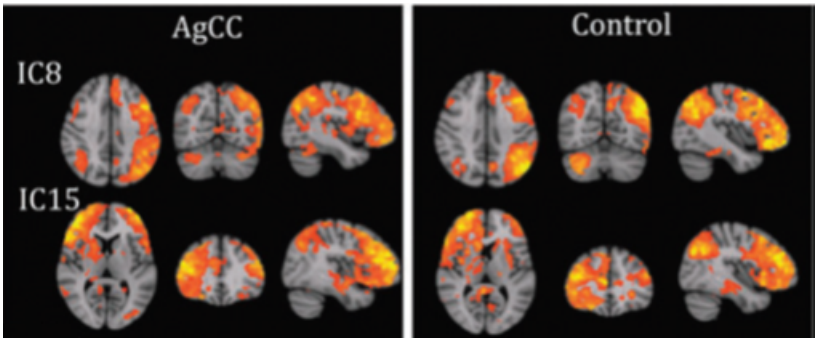

FIGURE 2.12: Qualitative comparison of two Resting-state state networks between AgCC and control. Adapted from Owen et al. [36].

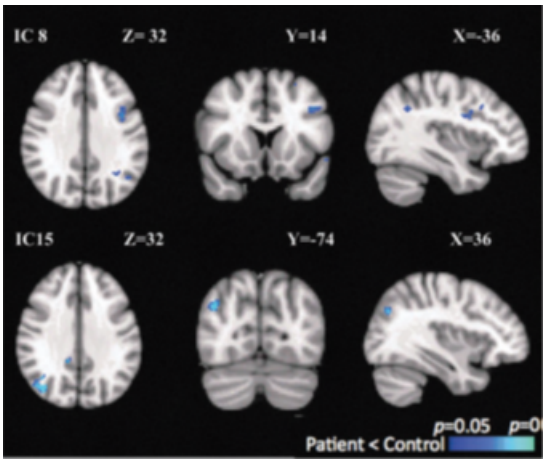

FIGURE 2.13: Quantitative differences of functional connectivity in AgCC versus controls for the same networks presented in fig. 2.12. Adapted from Owen et al. [36].

Another finding reports greater variability of functional connectivity for AgCC individuals (Table 2.1) than control [36], a result supported by the work described in the above paragraph where the same was true for the structural connectivity.

	Controls	*AgCC*	p-*Value*
Weighted all connections	0.40 ± 0.09	0.30 ± 0.07	7.4E-09
Weighted interhemi.	0.41 ± 0.10	0.29 ± 0.08	3.6E-19
Weighted intrahemi.	0.39 ± 0.08	0.31 ± 0.07	9.1E-13
Weighted intrahemi. (right)	0.41 ± 0.08	0.31 ± 0.08	5.7E-18
Weighted intrahemi. (left)	0.37 ± 0.10	0.31 ± 0.08	1.6E-06
Binary all connections	0.77 ± 0.02	0.74 ± 0.02	2.0E-07
Binary interhemi.	0.77 ± 0.02	0.74 ± 0.02	3.8E-20
Binary intrahemi.	0.76 ± 0.02	0.74 ± 0.02	4.8E-07
Binary intrahemi. (right)	0.77 ± 0.02	0.75 ± 0.02	9.5E-10
Binary intrahemi. (left)	0.74 ± 0.04	0.73 ± 0.03	0.003

TABLE 2.1: Edge space similarity. The increased variability of functional connectivity among AgCC individuals suggests rerouting of interhemispheric connections differs from person to person. Adapted from Owen et al. [36].

O'Reilly et al. [37] also investigated the effects of interhemispheric disconnection on functional networks, although focusing on the effects of sectioning the CC and Anterior Commissure on rhesus monkeys as opposed to studying AgCC individuals. Their results indicate a significant reduction in interhemispheric functional connectivity (fig. 2.14), both quantitative and qualitative, whereas Owen et al. [36] found the network qualitatively intact in AgCC.

The work of O'Reilly et al. [37] also supports the influence of commissures, other than the CC, on the cortical functional network. In fact they found that sectioning the CC but sparing the Anterior Commissure lead to preservation of interhemispherical connectivity (fig. 2.15). Indeed this result is in agreement with a prior

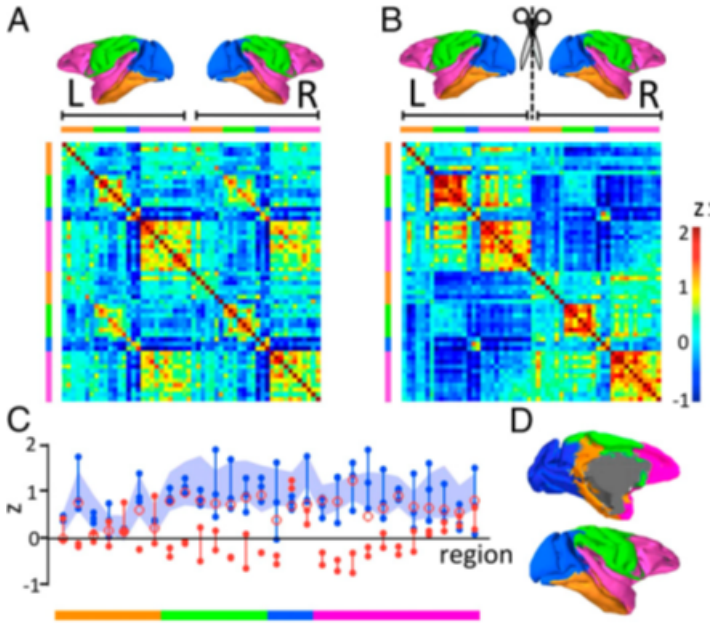

FIGURE 2.14: (A, B) Connectivity matrices for pre-section and post-section. Matrices are presented so that the main diagonal shows the correlation of each region with itself, the upper left and lower right quadrants show correlations within hemispheres, and the lower left and upper right quadrants show interhemispheric connectivity. (C) Fishers z correlation between homotopic regions. The shaded area is the mean 2 SD for a group of 18 control monkeys. In blue is depicted data from pre-section subject, post-section in full red and post-section with the AC spared in open red circles. (D) Location of the connectivity blocks that match the colored key above and beside each matrix. Adapted from OReilly et al. [37].

structural MR imaging study which shows an enlargement of the Anterior Commissure in 10% of AgCC individuals [38].

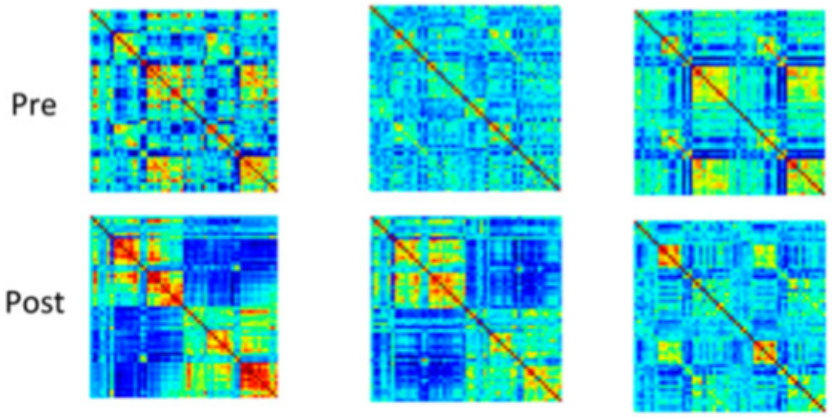

FIGURE 2.15: Connectivity matrices for pre-section and post-section for three different monkeys. The AC was sectioned in all subjects but (C). Matrices are presented in the same manner as in Fig. 14. Adapted from OReilly et al. [37].

Another important result from the research of O'Reilly et al. [37] shows an increase in intrahemispheric functional connectivity after CC+AC section and a small decrease for the same network in the case of CC only section (figs. 2.14 and 2.15). This last result seems to support the results of reduced intra-hemispheric functional connectivity in AgCC by Owen et al. [36].

All in all, these findings seem to validate the idea that, while the CC is responsible for most hemisphere to hemisphere connections in the healthy brain, the remaining commissures are capable of preserving its functions in its absence. In the next section we will review the model used to simulate the human brain.

2.3 Modeling the Human Brain

Over the last few years, we have watched a definitive trend towards obtaining experimental data via computer simulations. This has been the case as empirical tests become ever more costly and can be impractical as in the case of exploring the human brain's dynamics *in vivo*. As such many models have been developed and explored, namely the FitzHugh-Nagumo model, the Wilson-Cowan model and the Kuramoto model [10]. Models of this kind use abstraction (assumptions regarding the intrinsic spontaneous behavior of neural populations) to create a brain-inspired connectome, enabling a tractable neural network at the cost of lower spacial resolution.

With this in mind we chose this method of exploration with the goal of studying the effects of disconnecting the brain's hemispheres in incremental values, a difficult task using only empirical data. We achieved this by using a computational brain model developed recently which, although relatively simple to program, is capable of replicating large-scale neural network dynamics accurately, modeling human brain dynamics under rest and task conditions [1] [10] [39]. This model is based on the Kuramoto model and uses empirically obtained brain anatomical variables (connectivity patterns and grey matter sizes). We will review this model in full in this section.

2.3.1 Phase-oscillators

Before we begin describing the model used, the Kuramoto model of coupled oscillators and time delays, it is vital that the concept of oscillator is fully clarified. In general terms an oscillator is a system where the dynamics is represented by a single variable that varies over time and along a circular trajectory. Because this trajectory is a circle the variable in question has a determined range of possible

values and will return to the initial value after completing the loop. For convenience the periodic trajectory is often represented on the unit-circle. One of the possible variables used to describe the dynamics is the phase, which describes the position of any point in the periodic loop relative to a reference point. This is a variable that can be used in any oscillator model and is of great significance in this work as it is the one used in the Kuramoto model.

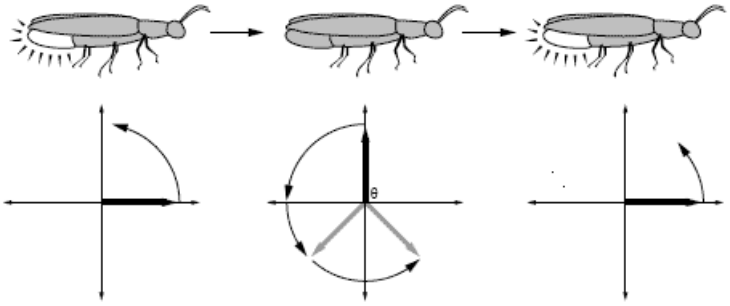

FIGURE 2.16: Fireflies as an example of system plausibly modeled by a phase oscillator.(https://www.learner.org/courses/mathilluminated/units/12/textbook/05.php)

The Kuramoto model is a network of phase-oscillators, with possible values in the $[-\pi, \pi]$ space. In the Kuramoto model the phase allows us to determine whether that oscillator is in synchrony with any other target oscillator by checking whether phase-lock was achieved. The evolution of the oscillators phase over time is described by ω_0, the oscillators natural frequency, which can be determined by:

$$\frac{d\theta}{dt} = \omega_0 \tag{2.1}$$

Next we will describe how the Kuramoto model can be used to represent brain dynamics.

2.3.2 The Kuramoto Model of Coupled Oscillators with Time Delays

As the title indicates, in this section we will describe the Kuramoto model of coupled oscillators with time delays, the model we used in this work to simulate the complex dynamics of the human brain. The version of the model we will review here was first developed by Cabral et al. [1], where it was shown to successfully simulate neural activity with a network of phase-oscillators.

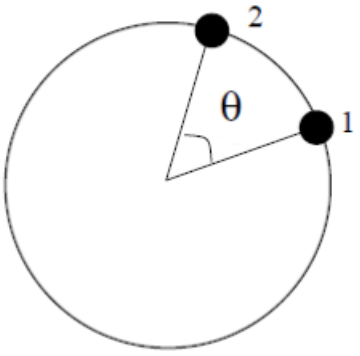

FIGURE 2.17: Schematic representation of two coupled phase oscillators. When phase locked, oscillator 2 leads oscillator 1 by a phase angle θ. Adapted from Bertrams lecture: Synchronization and Phase Oscillators.

As mentioned in the previous section on phase-oscillators, the Kuramoto model uses these as nodes, where each node represents a network of neurons, considered to be of homogeneous internal structure in the study we are reviewing. This approach was proven to be a valid representation of cortical rhythms as suggested by numerous studies, most notably in the works of Bartos et al.[40], Brunel and Wang [41] and Borgers and Koppell [42] where local neural networks have been shown to present gamma oscillations. The equation developed by Cabral et al [1] to simulate this network is as follows:

$$\frac{d\theta_n}{dt} = \omega_n + k\sum_{p=1}^{N} C_{np} sin(\theta_p(t-\tau_{np}) - \theta_n(t)) + \eta_n(t) \tag{2.2}$$

1) θ_n is the phase of the target oscillator (θ_p is the source) and their coupling is a periodic function, the *sin*;

2) ω_n is the target oscillators natural frequency;

3) k is the global coupling strength of the network, a measure of how strong the networks connections are;

4) C_{np} is the connectivity matrix, containing the connection strength between any two nodes;

5) L_{np} is the length matrix, containing the distance between any two nodes;

6) τ_{np} is the time-delay matrix, with the delay between the connections of any two nodes. This parameter is given by $\tau_{np} = \frac{L_{np}}{\nu} = \frac{\tau . L_{np}}{L}$, where v is the

connection speed, L is the mean fiber length and τ the mean delay of the network;

7) Finally, $\eta_n(t)$ represents the noise factor in the network.

This model represents the nodes influence on one another as a periodic function, the sine of the phase difference between two oscillators.

The first parameter shown in the equation above is ω_n, the oscillators intrinsic frequency that describes the natural evolution of its phase in the absence of external inputs, as described in the previous section. For this Cabral et al. [1] used a mean of 60Hz, assigned to each node according to a Gaussian distribution with standard deviation σ_f, as it was shown to be a plausible value for the resting-state dynamics [40] [41] [42].

Another concept needed to understand the model's functioning is the brain connectome, which was previously described in the Structural Networks section of this work, but for clarity purposes a brief summary will be provided here. The brain connectome used by Cabral et al [1] is built of both tractography data and brain parcelation. With brain parcelation various independent cortical regions are identified, in this case 66 different areas were created by the parcelation scheme [43].

From tractography data two matrices were obtained. One is the connection strength matrix, represented above as C_{np}, that contains data of the relative strength of connection between any source (p) and target (n) nodes (phase-oscillators). This is done by using the strength of tracts detected connecting both nodes. Although by this description it would seem that C_{np} is symmetrical it is important to note that this is not the case. This arises as the connection strength of any two nodes is calculated by dividing the total number of white matter tracts incoming to a node by the size of the region that node represents as determined by parcelation. Because the size differs from region to region in the network this results in a non-symmetric C_{np}, where the connection from p to n is different from n to p. Such a method of calculating the connection strength needs to be taken as the model needs to reflect the fact that a larger cortical region has more effect on a smaller one than in the reversed scenario [1]. With this approach, the higher the ratio of incoming axons to size, the stronger the connection to that area and,

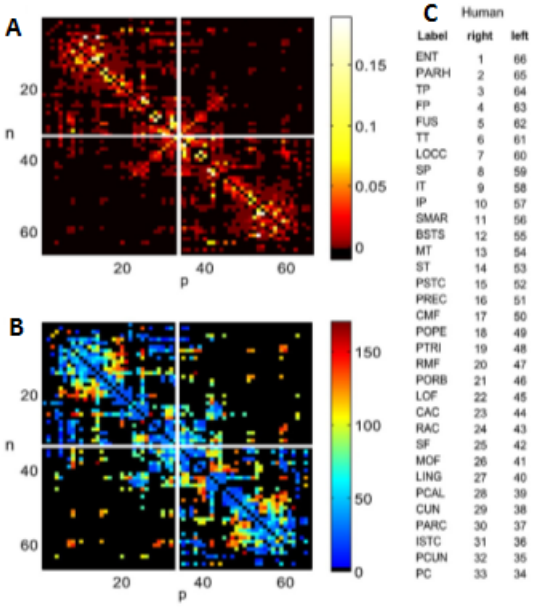

FIGURE 2.18: Structural connectome as developed by Cabral et al. [1]. (A) Connectivity matrix. (B) Fiber length matrix. Both matrices are arranged such that corresponding contra-lateral regions are symmetrically arranged with respect to the matrix center, the anti-diagonal revealing the existing connections between these contra-lateral regions. (C) Cortical region index. Adapted from Cabral et al. [1].

as consequence, its intrinsic activity is more strongly influenced by the external input.

The connectivity matrix, C_{np}, has a fixed structure and thus, the primary means of modulating this parameter was done through the global coupling weight of the network, represented in the equation as k. This global coupling weight is then very important as a free variable of the Kuramoto model, as it allows control over the scaling of connectivity strength and, as such, has been subject to an extensive exploration of its parameter space in the work we are reviewing. Their conclusions will be discussed after the theoretical background of the model has been fully detailed, in the next section of this chapter. Our own study of its parameter space will be presented in the Methods chapter.

The second matrix is the length matrix L_{np}, containing the information of fiber lengths connecting nodes p and n and thus the distances between them as well. This was calculated from tractography data as an average of the length of all fiber tracts connecting two nodes, with the intra-region lengths being set to 0. This data enters in the model equation show in (2.2) in the form of the time-delay, a parameter that describes the non-instantaneous nature of physiological connections. Unsurprisingly taking this into account is of vital importance in assuring the validity of a model of large-scale brain dynamics, where axons have

limited transmission speed, and variable axon myelination and synaptic processes impact the overall speed of the connection. This time-delay in the connection between two nodes is constructed with the mean length of fibers between those nodes of L_{np}, as mentioned, and conduction velocity v in the following manner:

$$\tau_{np} = \frac{L_{np}}{\nu} = \frac{\tau . L_{np}}{L} \tag{2.3}$$

This equation gives a delay matrix for the network, τ_{np}, with Cabral et al [1] choosing a value for v that is physiologically plausible as this parameter cannot be accurately determined. The value for v is given by $v = L/\tau$, where τ is the mean delay and L the mean fiber length. With the mean delay τ there is a factor that can scale the delays we impose on the network as a whole, meaning that this is another important free parameter of the Kuramoto model. Much like k we will review the exploration of its parameter space in the next section, whereas our own study is presented in the Methods chapter.

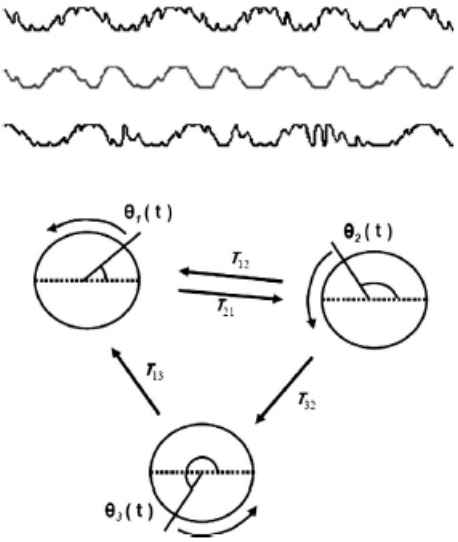

FIGURE 2.19: Graphical representation of three interacting oscillators with delayed coupling. (Bottom) Set of 3 coupled phase oscillators, with delayed interactions Tnp, where the angle on the circle represents the phase on the limit cycle of self-sustained neuronal oscillations. (Top) Example of 3 time series obtained from sin(n(t)). Adapted from Cabral et al. [44].

To finalize, there is the noise parameter,$\eta_n(t)$, which represents frequency dispersion and noise, contributing to a more accurate representation of the brains dynamics. For this Cabral et al. [1] used uncorrelated Gaussian white noise with zero mean and variance σ_n in radians. These are the final free parameters and their parameter space was investigated in the study and will be reviewed in the next sub-section.

2.3.3 Simulated Network Dynamics

As mentioned, all the results will be reviewed in this sub-section, but first there is need to understand how they were obtained and measured. The most important variables through which we can describe the evolution of the network dynamics over time are the Order Parameters. These measure global network synchrony and were first derived by Kuramoto:

$$R(t)e^{i}\phi(t) = \frac{1}{N}\sum_{n=1}^{N} e^{i}\theta_n(t) \tag{2.4}$$

The Order parameters $R(t)$ and $\phi(t)$ measure the phase uniformity and the movement of the oscillators around the limit circle respectively. $R(t)$ in particular is very useful when characterizing the networks dynamics as it can describe any state between a fully synchronized network, with $R(t) = 1$, and an incoherent state of the network where all the oscillators are desynchronized, for $R(t) = 0$.

The order parameter $R(t)$ also allows for two other descriptors of the global dynamics, the average of $R(t)$ simulated over time and its standard deviation. The first allows for a description of the global synchrony of the network referred to as Synchrony. The standard deviation of $R(t)$ (hereafter referred to as Metastability) describes how stable the networks synchronous states are, with high standard deviation representing a network with high variation, where synchrony may be high but never stays so for long. This describes a network with high Metastability [1].

We now know how Cabral et al. [1] simulated and evaluated neural activity with a network of phase-oscillators but there is still a need to understand how these results were compared to empirically-obtained results. The first step in this process is to convert the simulated data into BOLD for which the Balloon-Windkessel hemodynamic model, as described in Friston et al. [45], was used.

With the hypothesis that the variations in the oscillators phase are the root triggering the BOLD signal, Cabral et al. [1] used a Balloon-Windkessel model analogue to a linear filter and their results indicate that the correlations obtained depend only on the simulated network, i.e. with no influence of the hemodynamic model. The data they presented to verify these conclusions were adapted into fig. 2.20.

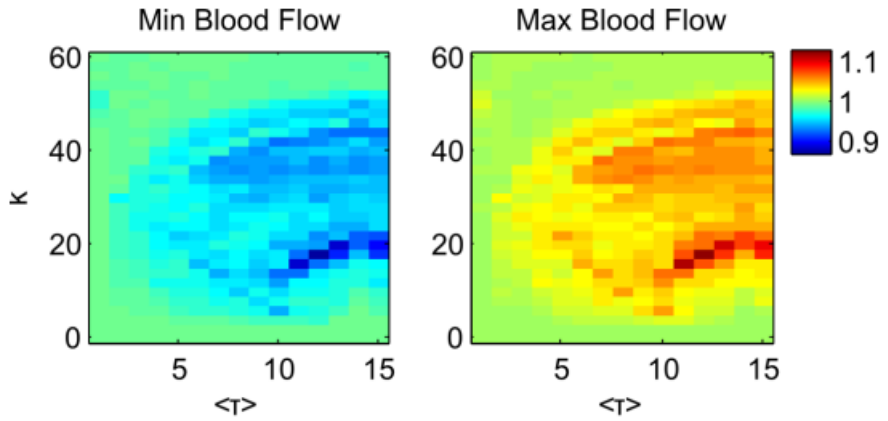

FIGURE 2.20: Diagrams representing the minimum value (left) and the maximum value (right) of the blood flow as a function of the mean delay τ, and the coupling strength, k. The blood flow fluctuates 15% at most. This means that the Balloon model is behaving essentially linearly, proving that the patterns we observe at the BOLD level come essentially from the network dynamics. Adapted from Cabral et al. [44]

The BOLD data provided by this model was then filtered to remove the high frequency components of the signal, increasing its physiological precision and eliminating possible incorrect correlations due to these components. For the last step in obtaining model results comparable to empirical FC Cabral et al.[1] obtained the BOLD signal for each area and calculated the correlation matrix by doing Pearsons correlation between paired areas. In doing so the simulated FC was created, and could be compared by means of a Pearson correlation with the analogous empirical FC.

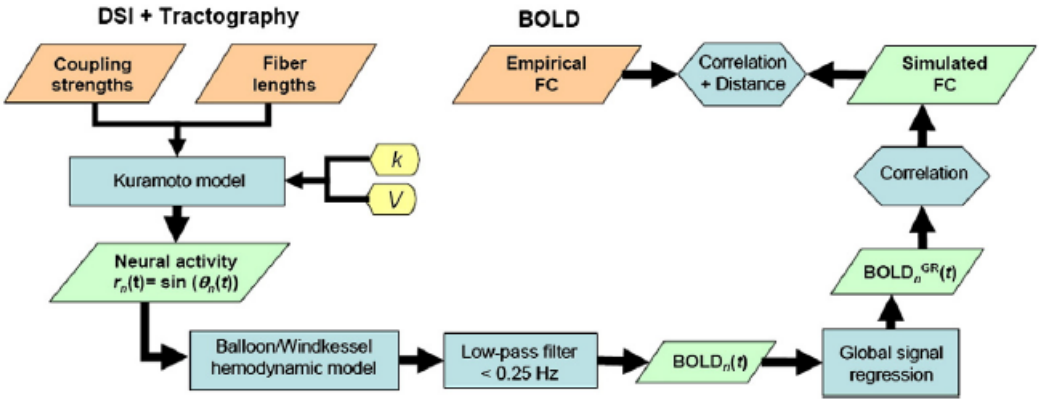

FIGURE 2.21: Flowchart illustrating the workflow from the empirical SC to simulated FC. Adapted from Cabral et al. [44]

Now we can describe the results obtained by Cabral et al. [1], which show this is a model capable of effectively simulating functional connectivity at rest. One of the major results from this study is the relatively small influence of both frequency

dispersion and noise. In this study they found that the model reacts most sensitively to changes in the (k, τ) plane. Indeed, whether considered simultaneously or separately, in the physiologically plausible range, the effect of changes to frequency dispersion and noise were minor and for every parameter combination tested, the network dynamics were preserved. Therefore, they decided not to include noise or frequency dispersion in the model.

Another result from this study was in accordance with previous work, where Acebron et al. [46] characterize the network dynamics of the Kuramoto model for a large number of nodes ($N \to \infty$) as a function of the global coupling k. These results are illustrated in the fig below in which a critical value of the global coupling (k_c) is evident. In this study, Cabral et al. [1] present a similar behavior in their results with a finite-sized network. For such a network, although $R(t)$ never exhibits a null value, there is a smooth but significant transition as the global coupling increases past its critical value ($k > k_c$), where $R(t)$ increases.

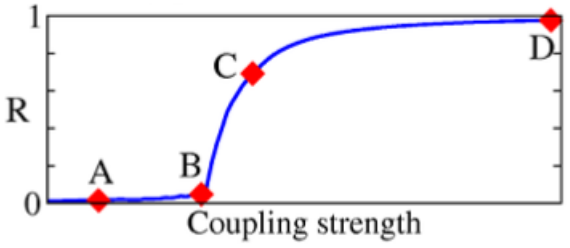

FIGURE 2.22: Order parameter R versus the coupling strength. Adapted from Popovych et al.[47]

Their results were also in agreement with the theoretical study by Lee et al.[48], indicating that as the mean delay, τ_{np}, increases, the network needs higher coupling values to maintain synchrony. This result is shown in fig. 2.23.

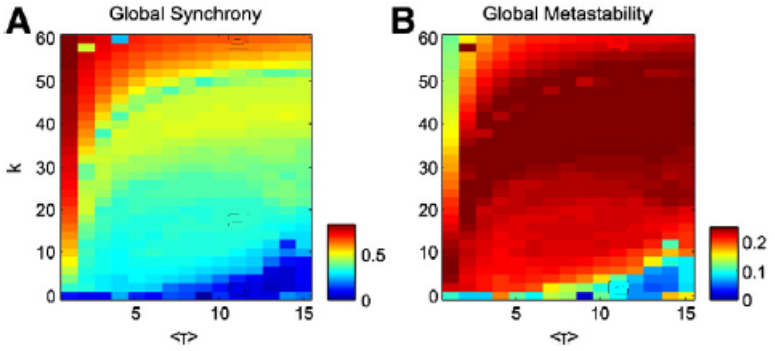

FIGURE 2.23: Global dynamics of the mean delay τ and coupling strength parameter space k. Adapted from Cabral et al. [44].

One additional result shows that $R(t)$ is seldomly found to be stationary. This indicates constant change in the network, with frequent transitions in the global

synchrony. Indeed, for a high enough global coupling but still bellow k_c it is revealed that Metastability is at its highest. In this state $R(t)$ exhibits very high variation and the network dynamics are at their most irregular, a result that agrees with the work done by Popovitch et al. [47]. As seen in fig. 2.24 this is a region where dynamic clusters of nodes appear, where a node may be synchronized to a cluster but not to the rest of the network.

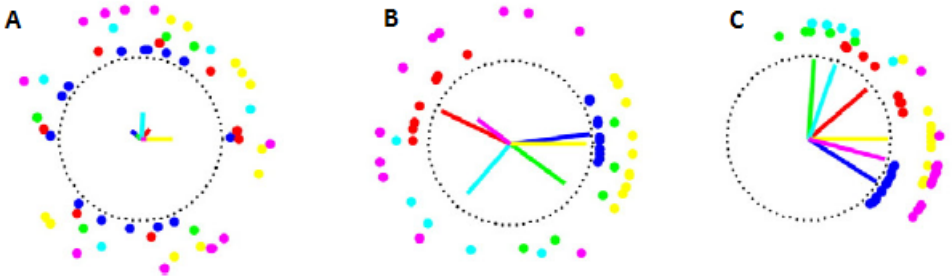

FIGURE 2.24: Snapshot of node phases for k=2, 18, 60. As k increases nodes go from incoherence (A) to cluster formation (B) to global synchrony (C). Adapted from Cabral et al. [44].

To finalize, Cabral et al. [1] also show that for the simulation parameters that maximize the correlation between simulated FC and empirical FC, the correlation between simulated FC and SC (Structural Connectivity) is high. This suggests that high Metastability, and SC and empirical FC correlations are all valuable indicators of the optimal parameter pair (k, t).

To summarize, the Kuramoto model of coupled oscillators here described replicates large-scale brain dynamics using a network of N oscillators. Each of these is a node that represents a neural network within a cortical region. It does so by simulating the variation in phase of a given target node n over time. This variation is affected by the multiple parameters we used, both intrinsic and extrinsic to the node. The intrinsic parameter is ω_n, the oscillators intrinsic frequency, which represents the phases natural evolution over time and with no external influences. The first extrinsic parameter we examined was the connectivity matrix,C_{np}, representing the strength of the connection between any two nodes and, as such, the influence the source exerts on the target node (if any). The next one was k, the global coupling weight of the network, which allows for scaling of the total influence that one node exerts on another and is, as such, an important free variable in this model. The other important free parameter we used was the mean delay of the network, τ_{np}, which allows for scaling the delay when two nodes communicate.

As a simplistic example, with no delay, if two nodes had the same phase the source would exert maximum influence on the target, as $sin(0) = 1$. By adding delay we

add frustration to the network, meaning that it is harder for two nodes to achieve phase-lock (synchronization). This is the case because, assuming two nodes with equal phases at time t, after taking delay into consideration the target would be receiving the influence of the source from the time $t - \tau_{np}$, when the source had a different phase. This scenario would make synchronization harder. As a final note in this summary the noise parameter was ignored for the reasons explained above.

Chapter 3

Methods

3.1 Structural connections

The structural connectivity data we used was empirically obtained and described by Cabral et al. [49]. This data was obtained using the magnetic resonance images from the brains of 21 healthy contributors (11 males and 10 females, ages: 22−45 years) with the use of diffusion tensor imaging (DTI). Afterwards anatomical connectomes were constructed for each individual using a tractography algorithm and, with the use of the automated anatomic labelling (AAL) template [50], the entire brain was parcellated into 90 regions each representing a node in the network.

With this data two 90x90 coupling matrices were created, C_{np}, the connectivity matrix and L_{np}, the length matrix. L_{np} was calculated as the Euclidean distance between any two nodes, n and p ,(each of the 90 nodes were placed at the centers of gravity of the respective brain area), with the intra-region lengths being set to 0. C_{np} contains the coupling strengths between any two regions n and p, where this connection strength is proportional to the number of fibers incoming to region n and the size of that region obtained from the tractography algorithm. However, the connectivity matrix is not symmetric as the connection from p to n is different from n to p (please see Chapter 2 for more detail).

In order to create a matrix capable of reliably representing the anatomical organization of the cerebral cortex of the whole group, the matrices were averaged across all subjects. For more detail on the steps necessary to create this data please refer to Chapter 2.

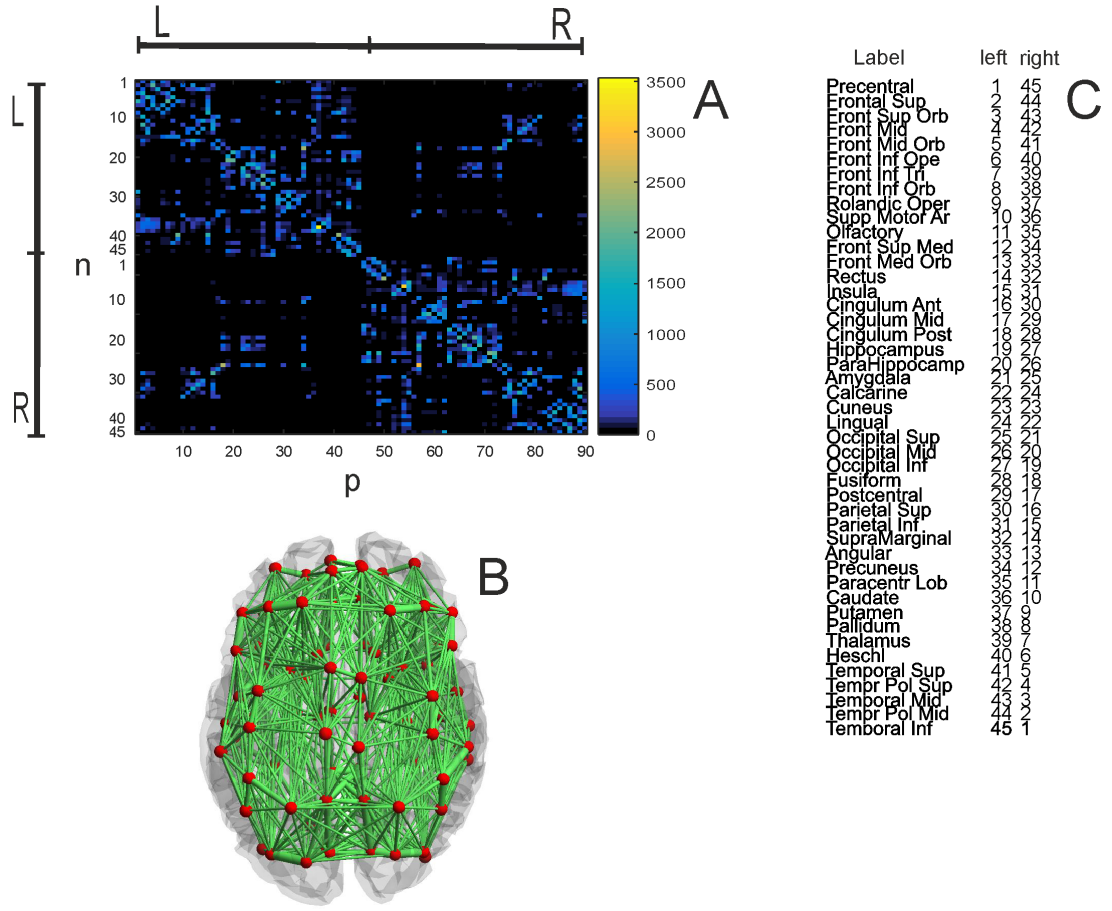

FIGURE 3.1: Structural matrix (A), connectome of the intact brain (B) and label for each of the 90 nodes(C).(A) The matrix is arranged so the main diagonal shows the connection of each region with itself, the upper left and lower right quadrants show the connectivity within hemispheres, and the lower left and upper right quadrants show interhemispheric connectivity. The source is n and p the target region. (B) The connectome is an above view of the brain with the frontal lobes closest to the bottom. The red nodes represent anatomical regions placed at their center of gravity coordinates.

3.2 Modeling Neural Dynamics

In order to simulate spontaneous brain activity we used the Kuramoto model of coupled oscillators with time delays [1] as described in Chapter 2. But, for clarity purposes, a much briefer description of the model we used is presented here. This model represents multiple brain regions as phase oscillators with an average intrinsic frequency in the gamma-band and describes the relationship of these oscillators in the network. The Kuramoto model we used is represented in the following expression:

$$\frac{d\theta_n}{dt} = \omega_n + k\sum_{p=1}^{N} C_{np} sin(\theta_p(t-\tau_{np}) - \theta_n(t)) + \eta_n(t) \tag{3.1}$$

Each variable represents a different characteristic of the network:

1) θ_n is the phase of the target oscillator (θ_p is the source) and their coupling is a periodic function, the *sin*;

2) ω_n is the target oscillators natural frequency;

3) k is the global coupling strength of the network, a measure of how strong the networks connections are;

4) C_{np} is the connectivity matrix, containing the connection strength between any two nodes;

5) L_{np} is the length matrix, containing the distance between any two nodes;

6) τ_{np} is the time-delay matrix, with the delay between the connections of any two nodes. This parameter is given by $\tau_{np} = \frac{L_{np}}{\nu} = \frac{\tau . L_{np}}{L}$, where v is the connection speed, L is the mean fiber length and τ the mean delay of the network;

7) Finally, $\eta_n(t)$ represents the noise factor in the network.

The process and reasoning behind selecting the values for each of the model parameters is discussed below in Model Parameter Determination. This model was then simulated with MATLAB (www.mathworks.com) using a script provided by Joana Cabral, (Postdoctoral Researcher, Department of Psychiatry - University of Oxford). The results of this model are measured using the Order Parameter $R(t)$ which describes phase uniformity (synchrony) between any two oscillators over time, varying between 0 and 1. To further the analysis of the simulation two other descriptors are used, Synchrony (average of $R(t)$) and Metastability (standard deviation of $R(t)$). Each of these is further described in Chapter 2.

3.3 Simulated BOLD and FC

In order to compare the simulation results with physiological data they need to be converted into a BOLD signal. To do so we used the Balloon-Windkessel model described by Friston et al. [51] [45]. This simulated BOLD signal was low-pass filtered bellow 0.25Hz to remove incorrect BOLD data and reduce the flaws of

hemodynamic model and then downsampled to achieve the same resolution as a MR scanner. The simulated Functional Connectivity was computed using Pearson correlation between the BOLD signals of any source and target nodes. This resulted in a 90x90 FC matrix with the information of all nodes in the network.

All calculations were done with MATLAB (www.mathworks.com) using a script provided by Joana Cabral (Postdoctoral Researcher, Department of Psychiatry - University of Oxford).

3.4 Model Parameter Determination

As described before, the Kuramoto model, like most models, has optimal parameters in order to achieve the most accurate representation of the human brain. One of such parameters is the oscillators' average intrinsic frequency, for which we used 40 Hz as it has been shown to result in an accurate representation of brain function [39]. Regarding the connectivity and length matrices, the method through which they were obtained is described in Chapter 2.

The remaining parameters are the principal descriptors of the network dynamics: the global coupling strength k, the mean delay of the network τ and the noise factor in the network $\eta_n(t)$. However, as shown in the characterization of the network behavior by Cabral et al. [1], the shift between incoherence and synchrony is most sensitive to the (k, τ) dimensions of this parameter space than to the noise, as $\eta_n(t)$, in its plausible biological range, has too little impact on the networks dynamics to justify a simulation in the complete parameter space. With our tests providing fundamentally the same results as this study, we opted to ignore the influence of this parameter and focus on the main descriptors of the model, (k, τ) in order to reduce the computing cost of the model.

To finalize we needed to identify the optimal values for (k, τ) and so, before truly utilizing the model, this parameter pair space was studied in order to find the parameters that best described the brain dynamics of the subject data we had available.

A good indicator of a suitable parameter pair is a high value of Metastability (the standard deviation of the order parameter, previously described in Chapter 2). High values of Metastability are mainly associated with an intermediate dynamical

regime where the coupling between areas is only sufficiently strong to form partially synchronized clusters, never reaching full synchronization. This regime occurs between incoherence and global synchronization due to the high heterogeneity and complexity of the structural connectome (couplings and delays). Nodes within a cluster display correlated BOLD signal forming a functional network resembling what is observed in real resting-state data.

With that in mind we chose the pairs that both maximized the values of Metastability and had a good fit with both structural and functional connectivity data from healthy subjects. Doing this resulted in various well-adjusted pairs and of those we opted to utilize the pairs $(k = 7, \tau = 12)$, $(k = 7, \tau = 13)$ and $(k = 7, \tau = 14)$ for further study (see figs.3.2 and 3.3). However, it is important to note that the structural and functional connectivity data we used in this process was obtained from two different groups of healthy subjects. This was done because we lacked the two types of data from the same group but, while not ideal, there should not be any significant differences between average resting-state functional connectivity of groups of healthy individuals.

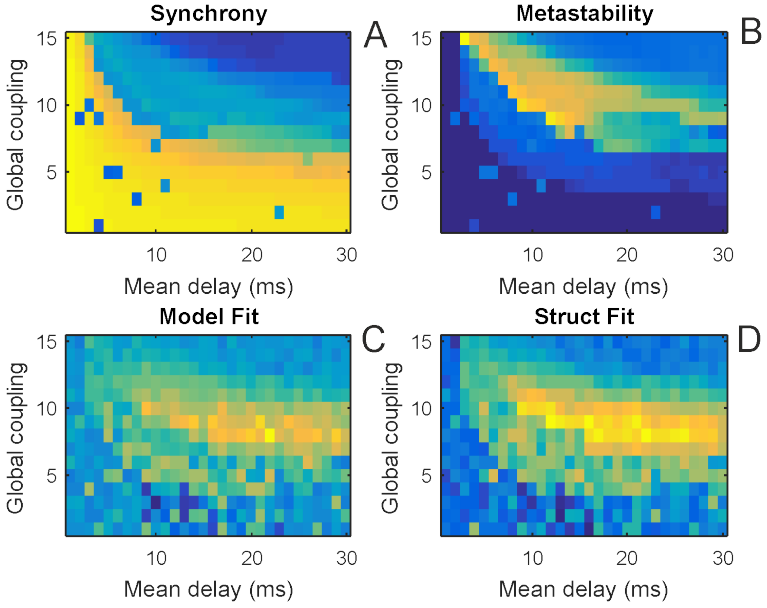

FIGURE 3.2: Exploration of parameter space (k, τ) for (A) Synchrony, (B) Metastability, (C) Functional Connectivity Fit and (D) Structural Fit.

3.5 Simulating Interhemispheric Disconnection

As described, neural networks in the model are connected according to the global coupling strength k and the coupling strength C_{np} matrix, forming the weighted

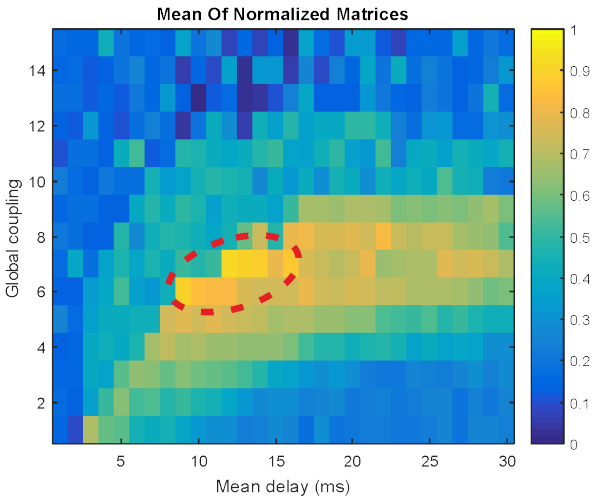

FIGURE 3.3: Determining the optimal pairs. To do so we normalized the relevant matrices from fig. 3.2 and averaged them, revealing the optimal pairs in the area inside the ellipse.

(connectivity) matrix K, where $K = kC_{np}$. Essentially, disconnection in the model implies that at least a subset of the weights K are reduced in comparison to the connected, healthy counterparts, which is done by altering the scaling done by k for this subset.

For this study two types of disconnection were utilized, one simulating the complete separation between the left and right hemispheres and another sparing the connections corresponding to the AC. For a description of interhemispheric connections and the structures that maintain them please refer to Chapter 2.

In order to implement total disconnection between hemispheres all interhemispheric connections in the structural connectome were identified and had all their weights decreased in equal proportion. This was achieved by defining a particular coupling strength for these connections, the interhemispheric coupling strength, which was done by multiplying the original interhemispheric connections, C_{np}, by a scaling factor ranging from zero to one. As such, we were able to model total disconnection with a scaling factor of zero and various partial interhemispheric disconnections with scaling factors between zero and one. The simulation where the AC is spared was done in a very similar fashion. The difference is merely in that the interhemispheric connections in the structural connectome pertaining to the AC (Olfactory Cortex and Middle and Inferior Temporal Gyri) were spared, which allowed the modeling of preserving the AC in an otherwise complete disconnection. In a manner identical to the previous case, total disconnection is

simulated with a scaling factor of zero and partial interhemispheric disconnections with scaling factors between zero and one. All calculations were done using MATLAB (www.mathworks.com).

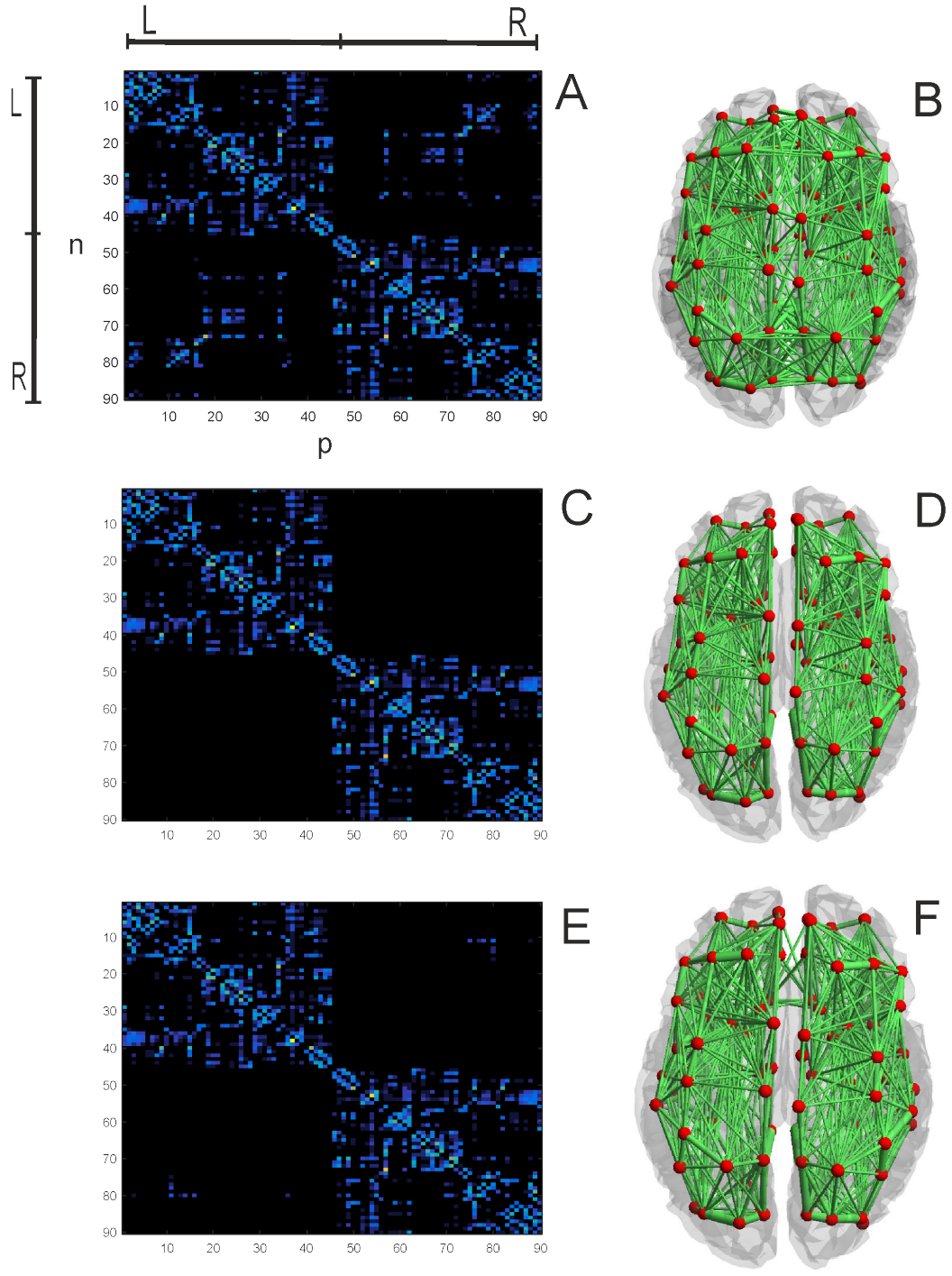

FIGURE 3.4: Structural matrix and connectome of the intact brain (A,B), Structural matrix and connectome of total corpus callosum section (C,D), Structural matrix and connectome of corpus callosum section sparing the Anterior Comissure (E,F). Matrices are presented in the same way as in fig.3.1(A).

Chapter 4

Results

4.1 Global Impact of Reducing the Strength of Interhemispheric Connections

In this section, we analyze the effect of the gradual reduction in the interhemispheric coupling strength on simulated resting-state functional connectivity measures. For this, we have simulated the functional connectivity matrices for the whole brain both for each of the three optimal model parameter pairs and for each of the various interhemispheric coupling strengths. The process through which this data was obtained is described in full in Chapter 3.

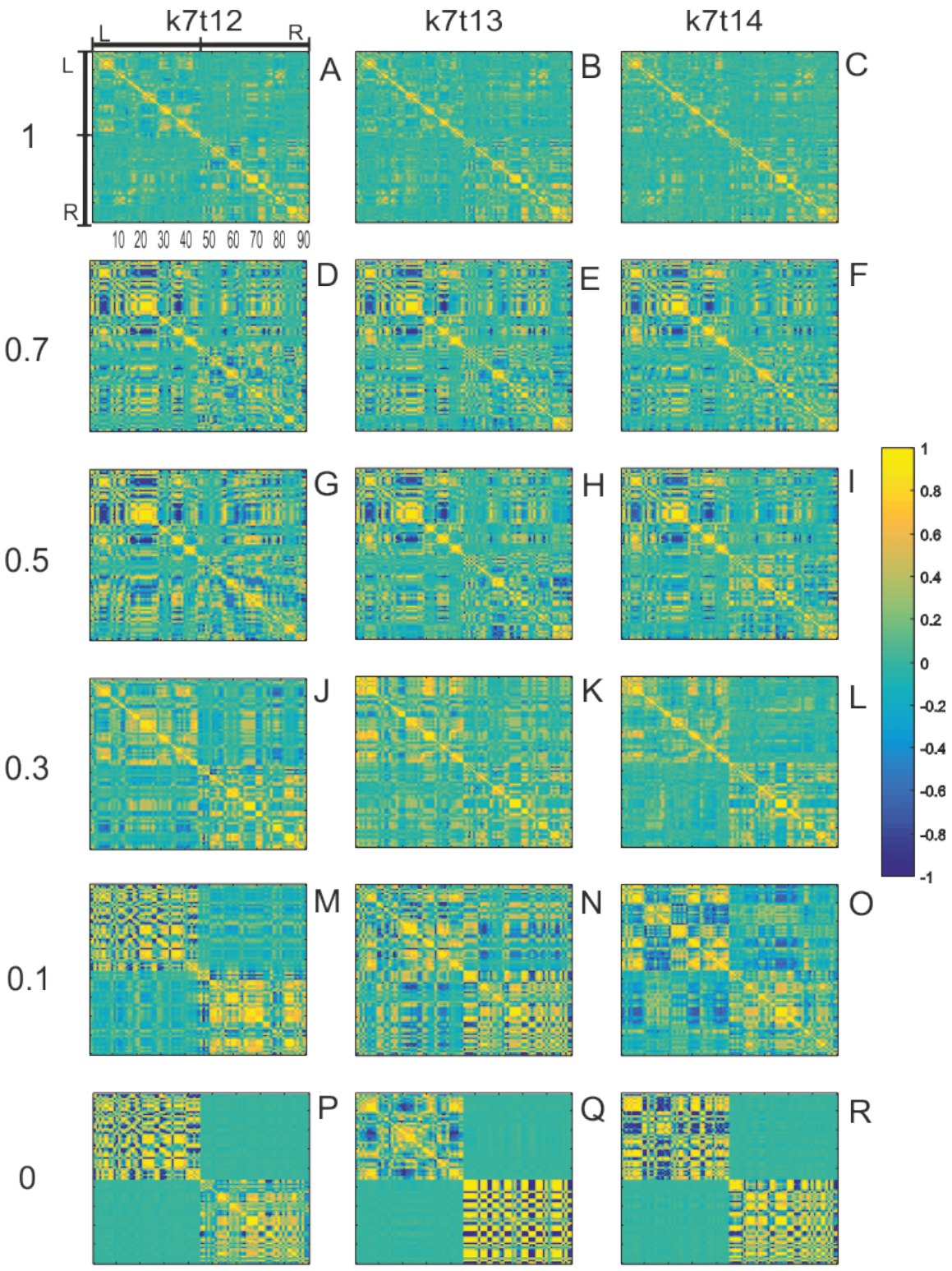

FIGURE 4.1: Matrices of functional connectivity (Pearsons Correlation between simulated BOLD signals in 90 areas) for three different sets of parameters (coupling strength k and mean delay τ) with decreasing strength of inter-hemispheric connections, from pre-lesion (Top) to complete corpus callosum section (Bottom). From left to right the mean transmission time (t in ms) increases from $\tau = 12$ to $\tau = 13$ and finally $\tau = 14$. The global coupling strength is kept constant at 7. From top to bottom, inter-hemispheric connections were scaled by a factor of 1 (no scaling A, B, C), 0.7 (D, E, F), 0.5 (G, H, I), 0.3 (J, K, L), 0.1 (M, N, O) and 0 (P, Q, R). Color scale ranges from $r = -1$ to $r = 1$ in all cases. Matrices are arranged so the main diagonal shows the correlation of each area with itself, the upper left and lower right quadrants show correlations within hemispheres, and the lower left and upper right quadrants show interhemispheric connectivity.

A clear conclusion from the results in fig.4.1 is the existence of a definitive influence of the interhemispheric structural connections in resting-state functional connectivity. The overall reduction in their strength is only significantly pronounced in the case of complete section for each parameter pair in fig3.1(P, Q, R). Although there are some reductions in the strength of interhemispheric connections for scaling factor values under 0.5, the strength of such connections apparently increased for scaling factor values between 1 and 0.5.

Another possible inference from fig.4.1 is the apparently increased intrahemispheric correlation as the scaling factor is reduced beyond 0.7. This is most evident in figs.3.1(M, N, O), when comparing to (A, B, C), where the increase is noticeable inside the left and right hemispheres. However, we find that in some cases this seems not to manifest, in particular in fig.4.1(K,N).

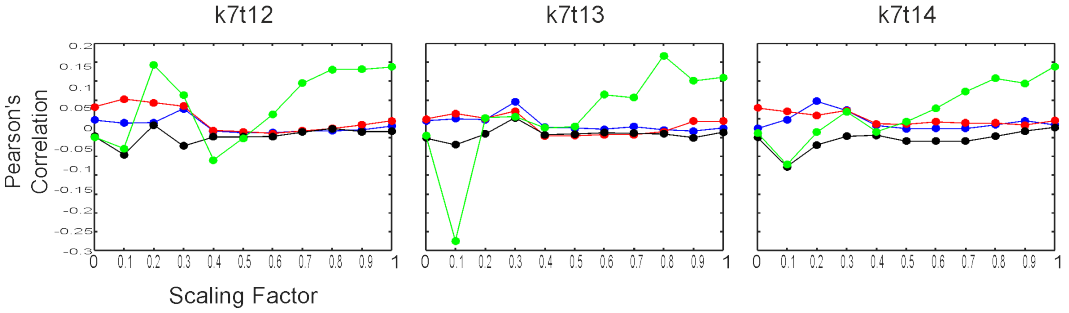

FIGURE 4.2: Average Pearsons Correlation for intrahemispheric, interhemispheric and homotopic connections, for each scaling factor. From left to right the mean transmission time (t in ms) increases from $\tau = 12$ to $\tau = 13$ and finally $\tau = 14$. The global coupling strength is kept constant at 7.The left hemisphere is depicted in blue, the right in red, interhemisferic connections in black and homotopic connections in green

From fig. 4.2 we can clearly note that the strongest correlation for pre-section (scalling factor 1) occurs for the homotopic connections.

4.2 Impact on Interhemispheric Connections

An immediate result of the changes caused by the reduction in the interhemispheric coupling strength is the influence in the connections between both hemispheres and, as such, a thorough study of such influence is essential. To do so we have produced graphics detailing the average correlation for each coupling strength in the interhemispheric connections, with special interest in the homotopic regions.

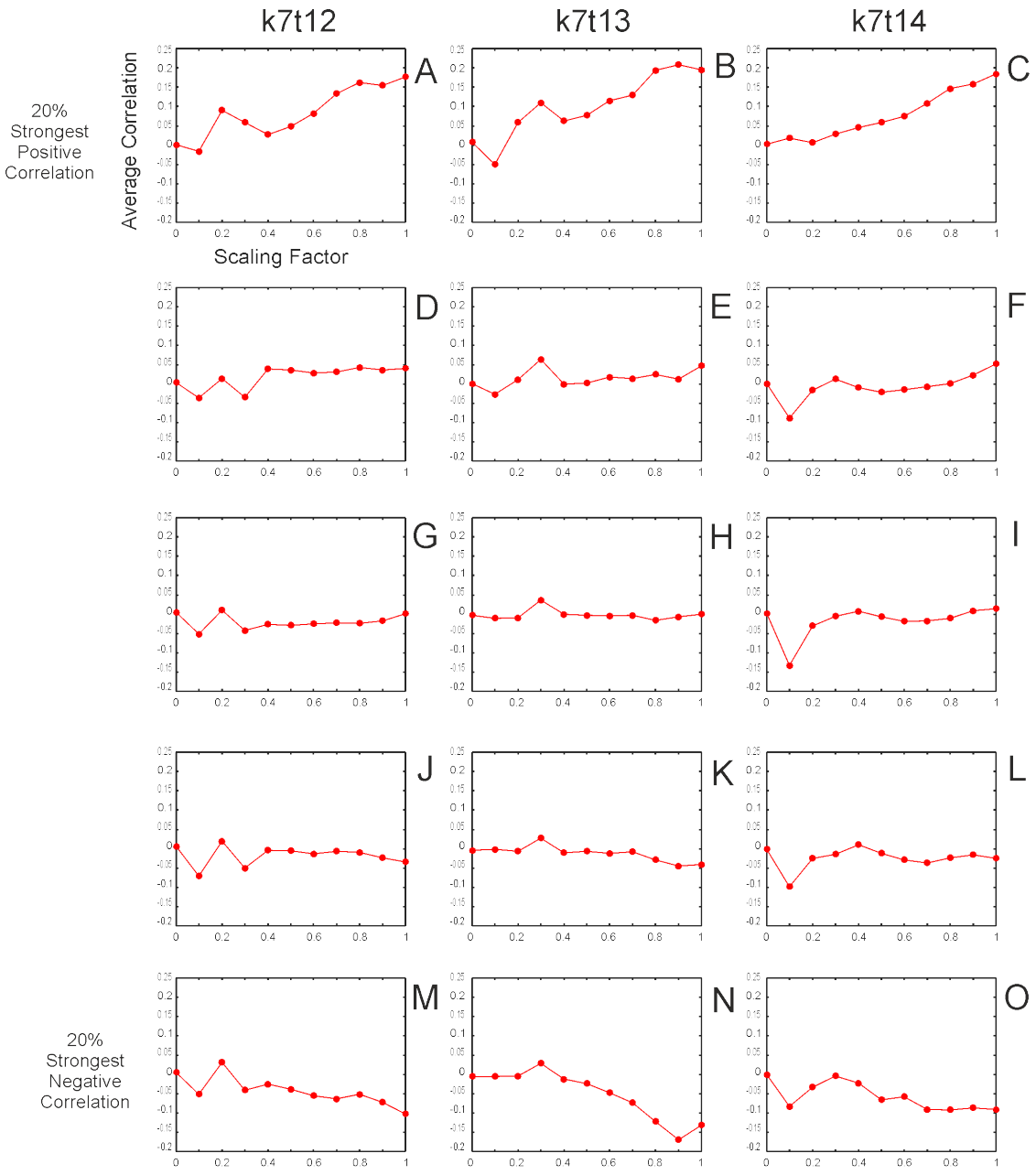

FIGURE 4.3: Average Pearsons Correlation in the interhemispheric connections for various groups, from the 20% strongest positive (Top) to the 20% strongest negative (Bottom), for each scaling factor. From left to right the mean transmission time (t in ms) increases from $\tau = 12$ to $\tau = 13$ and finally $\tau = 14$. The global coupling strength is kept constant at 7.

Next, we studied how, in our model, interhemispheric functional connectivity was affected by reducing the strength of interhemispheric structural connectivity, in groups of pairs of areas showing different levels of correlation in the intact brain, i.e., we divided the interhemispheric connections in 5 quintiles according to the strength of functional connectivity in the model with intact interhemispheric connectivity, from the 20% stronger connections (correlation) to the 20% most negative connections (anticorrelation). From fig.4.3 we can observe that the average

correlation for the interhemispheric connections tends to zero for each parameter pair, regardless of the group. Quintiles 20-40%, 40-60% and 60-80% present relative stability as the scaling factor diminishes. This observation suggests that interhemispheric connections that show weak functional connectivity in the intact brain, continue presenting weak connectivity when interhemispheric structural connectivity is reduced. There are, however some notable cases, particularly in the $k = 7\tau = 12$ and $k = 7\tau = 14$ parameter pairings where there is a noticeable variance for the scaling factor 0.1 and in the case of $k = 7\tau = 12$ for 0.2 also. For the $k = 7\tau = 13$ pair this occurs in the 0.3 factor. This is present in virtually every group and parameter pair, even occurring for the 40-60% group, a group that otherwise presents very low disparity.

Thus the main change observed in interhemispheric connectivity is restricted to the 20% of the connection showing stronger functional connectivity. These show a parametric reduction in their functional connectivity levels as interhemispheric structural connections are weakened.

Next we analyzed the 45 homotopic connections with the same method, by dividing them in quintiles according to the strength of their functional connectivity. As expected the average correlation for the homolotopic connections tends to zero as the scaling factor diminishes. There is also a noteworthy jump in the average correlation of each group for scaling factor 0.1 in parameter pair $k = 7$, $\tau = 13$ and 0.2 in $k = 7$, $\tau = 12$. The pair $k = 7$, $\tau = 14$ presents relatively low disparity with the exceptions seen in figs.4.4(O, L) where there is a slight decrease for the average correlation for scaling factor 0.1.

As observed in fig.4.5 the correlation between homotopic areas for scaling factor 0 is reduced to values close to zero in all areas.

4.3 Impact on Intrahemispheric Connections

To proceed with the detailed study of the changes brought by the reduction in the interhemispheric coupling strength, we also have to understand their influence in the connections inside each hemisphere. This is important because empirical data suggests that reducing interhemispheric connections enhances intrahemispheric functional connectivity [37]. With our model, we will be able to distinguish if

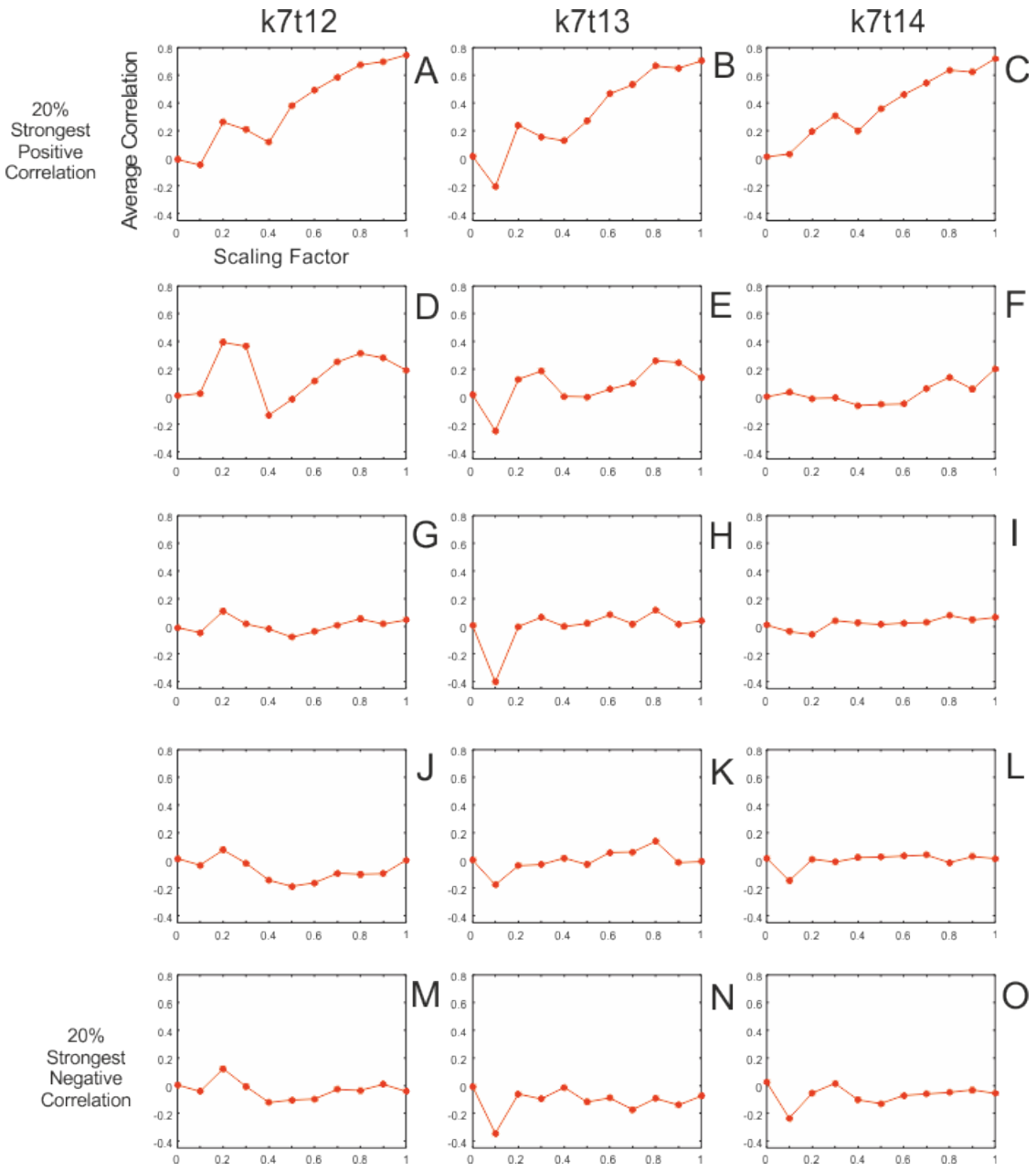

FIGURE 4.4: Average Pearsons Correlation in homotopic regions for various groups, from the 20% strongest positive (Top) to the 20% strongest negative (bottom) for each scaling factor. From left to right the mean transmission time (t in ms) increases from $\tau = 12$ to $\tau = 13$ and finally $\tau = 14$. The global coupling strength is kept constant at 7.

this could be a consequence of the structural alteration per se or if other underlying mechanisms are responsible for this increase like for example neural plasticity occurring after the interhemispheric lesion. As such, in this section, we present graphics detailing the average correlation for each coupling strength in both hemispheres.

In fig.4.6 we can confirm the relationship we detected previously in the intrahemispheric connections. The average correlation increases as the scaling factor

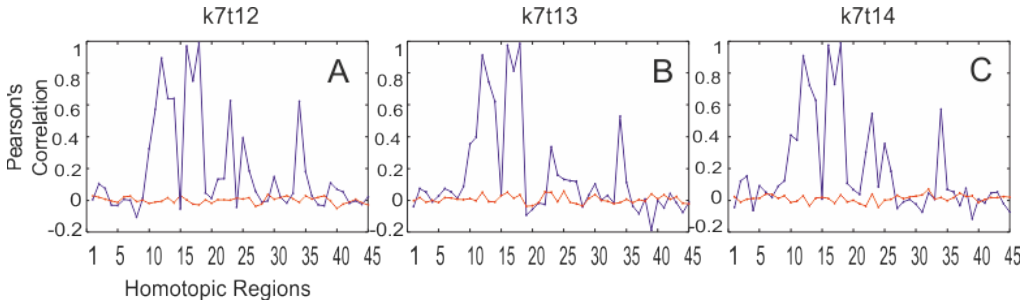

FIGURE 4.5: Pearsons Correlation for the homotopic areas for pre-section interhemispheric connections (scaling factor 1, in blue) and cut interhemispheric connections (scaling factor 0, in red), for each parameter pairing. From left to right the mean transmission time (t in ms) increases from $\tau = 12$ (A) to $\tau = 13$ (B) and finally $\tau = 14$ (C). The global coupling strength is kept constant at 7.

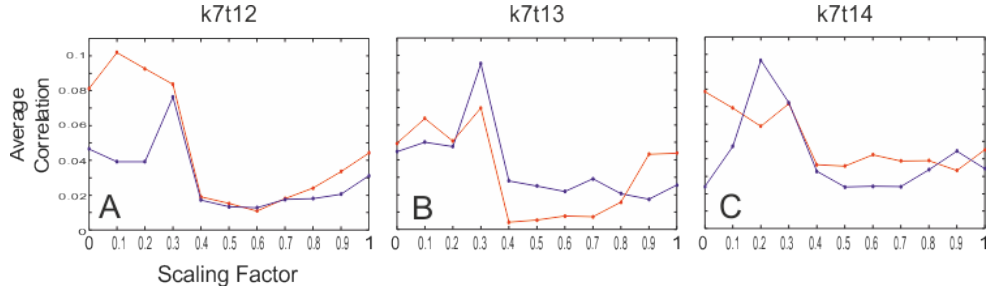

FIGURE 4.6: Average Pearsons Correlation in the left and right hemispheres for each scaling factor and for each parameter pairing. From left to right the mean transmission time (t in ms) increases from $\tau = 12$ (A) to $\tau = 13$ (B) and finally $\tau = 14$ (C). The global coupling strength is kept constant at 7.The left hemisphere is depicted in blue and the right in red.

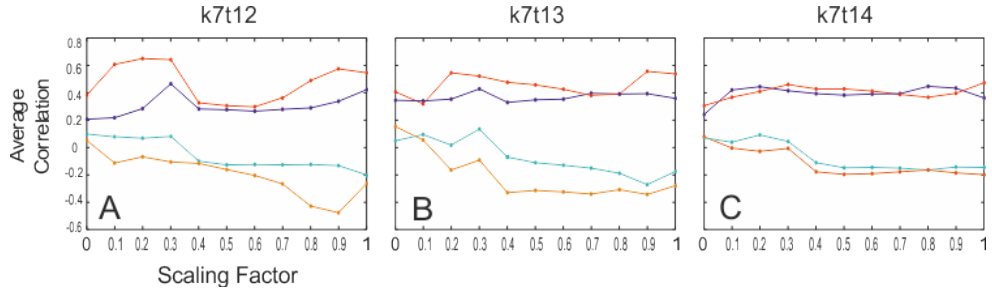

FIGURE 4.7: Average Pearsons Correlation for the 20% strongest positive and negative correlations in the left and right hemispheres for each scaling factor and for each parameter pairing. From left to right the mean transmission time (t in ms) increases from $\tau = 12$ (A) to $\tau = 13$ (B) and finally $\tau = 14$ (C). The global coupling strength is kept constant at 7. For the left hemisphere the strongest positive group is depicted in blue and the strongest negative in light blue. For the right hemisphere the strongest positive group is depicted in red and the strongest negative in orange.

is reduced beyond 0.4, surpassing the original correlation with scaling factor 1 in most cases. In fig.4.7 this relationship is further explored as either the strongest positive correlations increase for scaling factor 0.3 and below as seen in fig.4.7(A) for the right hemisphere or the strongest negative correlations approach zero for the same scaling factors as is most noticeable in fig.4.7(C). There is, however, one exception occurring on fig.4.6(C) for the pair $k = 7$, $\tau = 14$ in the left hemisphere for the scaling factor 0 where its correlation is slightly below the one for factor 1. Between the scaling factors 1 and 0.4 the average correlation usually diminishes

along the scaling factor with some exemptions.

Therefore, with our simulation data suggesting an increase in intrahemispheric functional connectivity when interhemispheric structural connections are reduced to 40% of their original strength, we hypothesize shuch alterations to be mostly due to the brain long-range structural connectivity. This is in line with empirical findings [37] but further research would help identify the cause of this phenomenon.

4.4 Impact of Reducing the Strength of Interhemispheric Connections on Specific Areas

Continuing our study, we proceeded with describing the behavior of specific homotopic connections of interest. To this end, we studied both the variation in correlation for each coupling strength as well as the pair of simulated bold signals for each connection. These homotopic connections were chosen as a window into the possible dynamics of a particular group of areas and as such we selected three areas, one with very high pre-section correlation (Posterior Cingulate Gyrus), one with almost no correlation (Middle Temporal Gyrus) and one with relatively high anticorrelation (Thalamus).

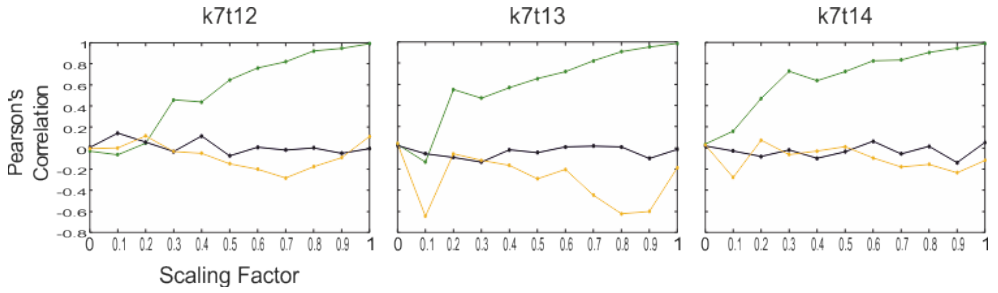

FIGURE 4.8: Pearsons Correlation in three homotopic connections for each scaling factor and for each parameter pairing. From left to right the mean transmission time (t in ms) increases from $\tau = 12$ (A) to $\tau = 13$ (B) and finally $\tau = 14$ (C). The global coupling strength is kept constant at 7. In green is represented an area with the strongest average of positive correlation for each pair (Posterior Cingulum), area with the lowest average in black (Middle Temporal Gyrus) and in yellow is depicted the area with the strongest average of negative correlation (Thalamus).

In fig.4.8 it is again clear the trend of diminishing correlation as the scaling factor decreases, in particular for the pair of areas showing stronger functional connectivity. That being said there is significant variation for the Thalamus connection in parameter pair $k = 7$, $\tau = 13$, in particular for scaling factor 0.1 and, to a slightly lesser extent, 0.8 and 0.9. We can also verify the existence of a critical scaling factor value. Beyond this point the region dynamics are changed, with a faster

decline of correlation. This observation is most obvious for the strongly correlated region in fig.4.8 (green).

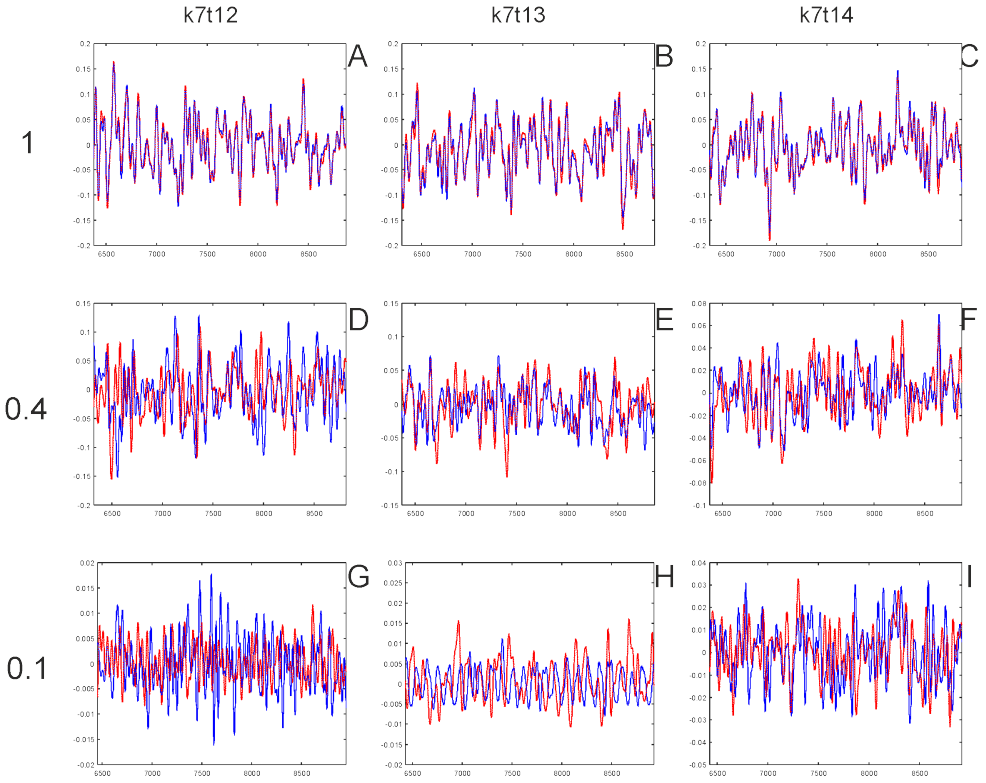

FIGURE 4.9: BOLD data in Posterior Cingulate Gyrus in a temporal interval for each scaling factor and for each parameter pairing. From left to right the mean transmission time (t in ms) increases from $\tau = 12$ (A) to $\tau = 13$ (B) and finally $\tau = 14$ (C). The global coupling strength is kept constant at 7. The left hemisphere is depicted in blue and the right in red.

In figs.4.9(A,B,C) we can see the strong overlapping of data which leads to the strong initial correlation for this pair of areas as represented in fig.4.8. This correspondence dies down as the scaling factor diminishes however, most notable in fig.4.9(H).

4.5 Sparing the Anterior Commissure

Interhemispheric connectivity is supported mainly by the corpus callosum connections and the anterior commissure. In order to separate the impact of each of these bundles of fibers, we simulated corpus callosum disconnection while leaving intact the anterior commissure. This would allow us to understand whether the results we observed can be attributed only to the severing of the corpus callosum. Indeed there is already evidence on the contrary with the results by OReilly et al. [37] showing a definitive influence of sparing the AC. To this end we simulated the

preservation of the anterior commissure in an otherwise complete cut allowing for comparison of interhemispheric connections after lesion.

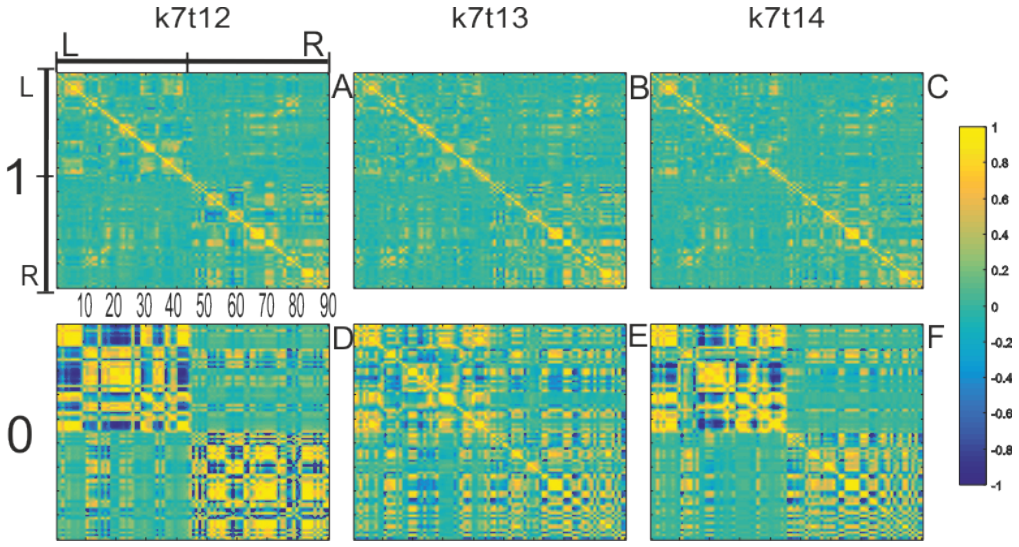

FIGURE 4.10: Matrices of connectivity (Pearsons Correlation) for each parameter pair, for pre-section (A, B, C) and complete section sparing the AC (D, E, F). From left to right the mean transmission time (t in ms) increases from $\tau = 12$ (A,D) to $\tau = 13$ (B,E) and finally $\tau = 14$ (C,F). The global coupling strength is kept constant at 7.Color scale ranges from $r = -1$ to $r = 1$ in all cases. Matrices are arranged so the main diagonal shows the correlation of each area with itself, the upper left and lower right quadrants show correlations within hemispheres, and the lower left and upper right quadrants show interhemispheric connectivity.

When the results shown in fig.4.10 (D, E, F) are compared with the ones shown in fig.4.1(P, Q, R), it is evident that sparing the AC led to the preservation of considerable interhemispheric connectivity after severing all other interhemispheric connections. It is also worth noting that, just as in fig.4.1, there seems to be an increased intrahemispheric correlation after the cut, particularly noticeable in figs.4.10 (D,F).

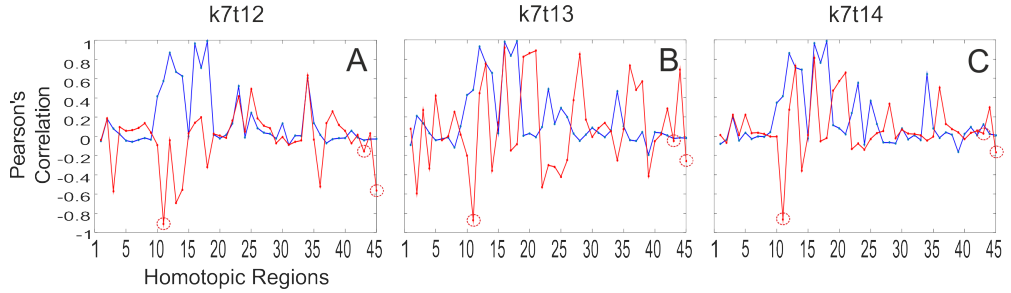

FIGURE 4.11: Pearsons Correlation for the homotopic areas for pre-section interhemispheric connections (scaling factor 1, in blue) and cut interhemispheric connections sparing the AC (scaling factor 0, in red), for each parameter pairing. As described in Chapter 3 the connections spared when simulating this lesion were connection 11, between the olfactory cortices, and connections 43 and 45, the middle and inferior temporal gyri respectively. From left to right the mean transmission time (t in ms) increases from $\tau = 12$ (A) to $\tau = 13$ (B) and finally $\tau = 14$ (C). The global coupling strength is kept constant at 7.

Building from the results presented in fig.4.10 and in fig.4.11 we can clearly see that the preservation of interhemispheric connectivity is not limited to the connections that were structurally preserved when simulating the lesion. Another interesting result presented in fig.4.11 are the clear changes from positive correlation to negative correlation or no correlation and *vice versa*, highlighting the importance of indirect structural connections in functional connectivity results. Furthermore, these results indicate that while, on average, connectivity may be preserved its overall pattern is definitively altered after the section.

Chapter 5

Discussion

In this chapter, we will present and describe the implications of the most significant findings of our work. These findings were three-fold: the model predicts a monotonic reduction in interhemispheric functional connectivity as the strength of structural connections diminish, an increase of intrahemispheric connectivity as the strength of structural connections diminish below 40% of their original value and a unmistakable preservation of functional connectivity after total section when the anterior commissure is preserved, albeit with important quantitative changes in the network.

Our model showed results consistent with previous interhemispheric connectivity studies. Namely our results in fig.4.1(P, Q, R) indicated a clear absence of interhemispherical connectivity post-section (using a scaling factor of 0), a result that, while expected, is confirmed in the work of OReilly et al. [37] where they used rhesus monkeys to study the effect of disconnection on interhemispheric functional connectivity. Indeed two other findings are in accordance with their research. With this model we presented evidence of a clear preservation of interhemispheric connections post-section when sparing the anterior commissure, a result which is consistent with the work done by OReilly et al. [37]. We also found an increase in intrahemispheric connectivity post-section for all parameter pairs and for complete section, with only one exception verified, in the case of the left hemisphere in pair $k = 7$, $\tau = 14$, (fig.4.6 A,B,C). However, when sparing the anterior commissure OReilly et al. [37] noted this increase in interhemispheric connections was much more subtle and at most barely significant. With our model we still noted

an increase in intrahemispheric connections when sparing the anterior commissure (fig.4.10b) but we did not study its significance due to time constraints.

As expected, our results also indicated higher average homotopic correlations with pre-section structural connectivity than either inter or intrahemispheric correlations fig4.2. This is corroborated by the work of Stark et al. [32] where they examine correlated activity between homotopic regions using fMRI data from healthy volunteers. However, results obtained with the Kuramoto model showed noteworthy differences in regional variation of homotopic correlation when compared to the results obtained by Stark et al. [32]. Our results present a reduced number of strong homotopic correlations but the regions presenting higher levels of correlation match the ones obtained empirically by Stark et al [32]. Discrepancies between the two results might be due to variations on fMRI data obtained for both studies and to the fact that ours is a simplified model of the human brain. Also, Stark et al [32] used a different brain parcellation scheme resulting in 56 homotopic connections in comparison with the 45 from our study. This is a restraint of working with a simplified model of the human brain. As we are approximating the dynamics of an entire cortical region to a simple phase oscillator, we cannot expect the model results to be faultless. Nevertheless, these results indicate that the Kuramoto model of Coupled Oscillators and Time Delays is able to qualitatively simulate resting-state interhemispheric homotopic connections albeit with quantitative disparities as the number of strong functional connections appears reduced.

Despite not having modeled callosal agenesis (AgCC) some parallelisms can be drawn between this work and the study by Owen et al. [36]. In their work on resting-state networks in AgCC they found that while qualitatively these networks presented no variation from the controls quantitative measures indicate definitive quantitative changes in functional connectivity for some intra-hemispheric and interhemispheric networks in subjects with AgCC. This result is somewhat mimicked in figs.4.10 and 4.11 where we show that sparing the anterior commissure preserved connectivity but with a definitive quantitative impact on the network dynamics. We have also found quantitative change in the cases where we reduce the strength of structural connectivity, as shown in fig.4.1 (D, E, F, G, H, I, J, K, L, M, N, O). This is true regardless of how small the structural damage may be, as presented in fig.4.1 (D, E, F), where even for a relatively small reduction in the

scaling factor (1 to 0.7) there is a significant impact on the functional connectivity. This furthers the already established notion that there is a significant causal link between structural and functional connectivity [37]. An interesting venue to explore would be to model AgCC using structural DTI data of subjects with the condition as it would allow further comparisons to be made. With our present model, we could predict how much the changes observed in patients with AgCC might be due to reduced interhemispheric connectivity.

Using this model we predicted a monotonic reduction in interhemispheric functional connectivity as the strength of structural connections diminish. This can be verified in figs.4.3 and 4.4 where we present the results on the interhemispheric and homotopic connections of particular quintiles. However we can also anticipate the existence of critical scaling factors for each quintile, a critical value on which the area dynamics change drastically, even if only for that particular value. We investigated this further with our study into specific homotopic connections (fig.4.8), where we verified that such a critical condition applies to each region individually. After that critical condition is reached it is clear that a change occurs in the regular dynamic of the region, leading to a faster decline of correlation. This is most evident in the case of the strongly correlated region (fig.4.8) where the regular decline in correlation is interrupted at a critical scaling factor value, regardless of parameter pair. In fact, we have already reported such a critical structural condition, where scaling factors below 0.4 led to an increase in intrahemispheric connectivity. In their work, OReilly et al. [37] speculate that increases in intrahemispheric connectivity may be somehow linked to the paradoxical findings in which functional connectivity between some regions increases for individuals with neurodegenerative diseases or in the early stages of such diseases. Whether this increase could be used as diagnosis for such diseases might be a compelling topic for further research. Additional exploration into the fluctuations in functional connectivity of each individual homotopic connection might have proven to be fruitful but with a limited time to complete this work we narrowed our search to those we considered to be the most illustrative.

In this thesis, we simulated *in silico* the changes in resting-state brain functional connectivity that would occur as interhemispheric connections are weakened, as such a study would be highly difficult to achieve in vivo. The greatest strength of a model as an investigative tool is also its weakness as, while it may allow researching previously untouched questions its results will always be predictions

while no other studies exist to confirm or contradict them. With this in mind we opted not to focus on a statistical analysis of our results as time-constraints forced us to shorten our research. Notwithstanding that, this research would certainly improve with such an approach but, as there are no studies to compare to, the increased complexity would amount to little gain.

During our work with this model our most significant restraint was the simplicity of the model itself, as, while it allows for a tractable simulation of neural dynamics, the assumptions we make when using the model lead to results that can only be used as rough estimates of what brain function really entails. This uncertainty is unavoidable in models of this kind as representing the dynamics neural populations as phase-oscillators with Euclidean distance connections will always be a large approximation to make. Another limitation of this work had to do with the data we used. Our structural connectome was acquired from 21 healthy subjects but as we did not have access to their functional connectivity data, we had to use data from another group of 16 healthy subjects in order to determine the optimal parameters of the model. While it certainly is not optimal, there should not be any significant differences between average resting-state functional connectivity of groups of healthy individuals, which we had to resort due to data not being available.

All in all, the Kuramoto Model of Coupled Oscillators and Time Delays presents results that are in line with previous research and, as such we believe it to be a valid and useful tool when investigating the cerebrum. Its simplicity comes with the disadvantage of uncertainty, but it is a fair trade when we consider the opportunity to research previously inaccessible characteristics of the human brain.

Chapter 6

Conclusion

To this day, complete understanding of the role that interhemispheric connections play on normal brain function remains an important scientific challenge. In this work we describe and utilize the Kuramoto model of Coupled Oscillators and Time Delays to provide further insight into their impact on resting-state functional connectivity. To do so we simulated the spontaneous behavior of brain areas coupled together in a large-scale network structure of the brain while systematically reducing structural interhemispheric connection strength. Our network structure was based on structural connectivity between 90 brain areas averaged across 21 healthy subjects. With this model we observed a clear monotonic reduction of interhemispheric functional connectivity as we diminish their structural connections. This result indicates a definitive influence of the brains structural connectivity on its functional networks, a conclusion that is supported by previous research. Our research also shows an increase in intrahemispheric functional connectivity as we diminish the structural strength of interhemispheric connections to values lower than 40% of their original strength. While the cause of such increase is still to be determined this result may help understand findings in in which functional connectivity between some regions increases in disease or pre-disease states. Another important finding relates to the preservation of functional connectivity when a small part of structural interhemispheric connections are preserved, the ones that represent the anterior commissure in vivo. However, despite maintaining functional connectivity, this corpus callosum only section led to significant quantitative changes in the functional network. This observation can be compared to previous studies of agenesis of corpus callosum where quantitative changes are reported despite the subjects presenting regular functional networks.

Building on previous research our findings also indicate the Kuramoto model of Coupled Oscillators and Time Delays as a valid tool for studying neural dynamics. Our study is far from exhausting the possible applications of this model in this field of research and, as such, there is plenty opportunity to further our work.

6.1 Further Work

To finalize the evaluation of the role of interhemispherical connections in resting-state functional connectivity we could proceed with the characterization of our findings using statistical and graph theory measures.

It would also be interesting to further our research by studying more homotopic connections as additional insights may be gained by their dynamics. Other venues to explore would be to model AgCC using structural DTI data of subjects with the condition and to discern whether increased functional connectivity could be used as diagnosis for neurodegenerative diseases by comparing our simulations with their fMRI data.

Bibliography

[1] Joana Cabral, Etienne Hugues, Olaf Sporns, and Gustavo Deco. Role of local network oscillations in resting-state functional connectivity. *NeuroImage*, 57 (1):130–139, 2011. ISSN 10538119. doi: 10.1016/j.neuroimage.2011.04.010. URL http://dx.doi.org/10.1016/j.neuroimage.2011.04.010.

[2] Olaf Sporns. The human connectome: A complex network. *Annals of the New York Academy of Sciences*, 1224(1):109–125, 2011. ISSN 00778923. doi: 10.1111/j.1749-6632.2010.05888.x.

[3] Steven L. Bressler and Emmanuelle Tognoli. Operational principles of neurocognitive networks. *International Journal of Psychophysiology*, 60(2):139–148, 2006. ISSN 01678760. doi: 10.1016/j.ijpsycho.2005.12.008.

[4] Anandamohan Ghosh, Y. Rho, a. R. McIntosh, R. Kötter, and V. K. Jirsa. Noise during rest enables the exploration of the brain's dynamic repertoire. *PLoS Computational Biology*, 4(10), 2008. ISSN 1553734X. doi: 10.1371/journal.pcbi.1000196.

[5] Olaf Sporns. Introduction. pages 247–262, 2013. ISSN 1958-5969. doi: 10.1137/S003614450342480.

[6] Martijn P. Van Den Heuvel, René C W Mandl, René S. Kahn, and Hilleke E. Hulshoff Pol. Functionally linked resting-state networks reflect the underlying structural connectivity architecture of the human brain. *Human Brain Mapping*, 30(10):3127–3141, 2009. ISSN 10659471. doi: 10.1002/hbm.20737.

[7] Martijn P. van den Heuvel and Hilleke E. Hulshoff Pol. Exploring the brain network: A review on resting-state fMRI functional connectivity. *European Neuropsychopharmacology*, 20(8):519–534, 2010. ISSN 0924977X. doi: 10.1016/j.euroneuro.2010.03.008. URL http://dx.doi.org/10.1016/j.euroneuro.2010.03.008.

[8] Martin a Koch, David G Norris, and Margret Hund-Georgiadis. An investigation of functional and anatomical connectivity using magnetic resonance imaging. *NeuroImage*, 16(1):241–250, 2002. ISSN 1053-8119. doi: 10.1006/nimg.2001.1052.

[9] Hae-Jeong Park and Karl J Friston. Structural and functional brain networks: from connections to cognition. *Science (New York, N.Y.)*, 342(6158):1238411, 2013. ISSN 1095-9203. doi: 10.1126/science.1238411. URL http://www.ncbi.nlm.nih.gov/pubmed/24179229.

[10] Joana Cabral, Morten L. Kringelbach, and Gustavo Deco. Exploring the network dynamics underlying brain activity during rest. *Progress in Neurobiology*, 114:102–131, 2014. ISSN 18735118. doi: 10.1016/j.pneurobio.2013.12.005. URL http://dx.doi.org/10.1016/j.pneurobio.2013.12.005.

[11] Olaf Sporns. Network attributes for segregation and integration in the human brain. *Current Opinion in Neurobiology*, 23(2):162–171, 2013. ISSN 09594388. doi: 10.1016/j.conb.2012.11.015. URL http://dx.doi.org/10.1016/j.conb.2012.11.015.

[12] Patric Hagmann. From diffusion MRI to brain connectomics. 3230:141, 2005. doi: 10.5075/epfl-thesis-3230. URL http://infoscience.epfl.ch/record/33696.

[13] Olaf Sporns, Giulio Tononi, and Rolf Kötter. The human connectome: A structural description of the human brain. *PLoS Computational Biology*, 1 (4):0245–0251, 2005. ISSN 1553734X. doi: 10.1371/journal.pcbi.0010042.

[14] Weisskoff RM Wedeen VJ, Davis TL. White matter connectivity explored by mri. In *Proceedings of the First International Conference for Functional Mapping of the Human Brain*.

[15] Brian J. Jellison, Aaron S. Field, Joshua Medow, Mariana Lazar, M. Shariar Salamat, and Andrew L. Alexander. Diffusion Tensor Imaging of Cerebral White Matter: A Pictorial Review of Physics, Fiber Tract Anatomy, and Tumor Imaging Patterns. *American Journal of Neuroradiology*, 25(3):356–369, 2004. ISSN 01956108. doi: 10.1038/nrn2776.

[16] Peter a. Bandettini. What's new in neuroimaging methods? *Annals of the New York Academy of Sciences*, 1156:260–293, 2009. ISSN 00778923. doi: 10.1111/j.1749-6632.2009.04420.x.

[17] N K Logothetis, J Pauls, M Augath, T Trinath, and a Oeltermann. Neurophysiological investigation of the basis of the fMRI signal. *Nature*, 412(6843): 150–157, 2001. ISSN 0028-0836. doi: 10.1038/35084005.

[18] S Ogawa and Tm Lee. Brain magnetic resonance imaging with contrast dependent on blood oxygenation. *Proceedings of the ...*, 87(24):9868–72, 1990. ISSN 0027-8424. doi: 10.1073/pnas.87.24.9868. URL http://www.pubmedcentral.nih.gov/articlerender.fcgi?artid=1262394&tool=pmcentrez&rendertype=abstract$\delimiter"026E30F$nhttp://www.pnas.org/content/87/24/9868.short.

[19] D a Gusnard, M E Raichle, and M E Raichle. Searching for a baseline: functional imaging and the resting human brain. *Nature reviews. Neuroscience*, 2 (10):685–694, 2001. ISSN 1471-003X. doi: 10.1038/35094500.

[20] Baxter P. Rogers and John C. Gore. Empirical comparison of sources of variation for FMRI connectivity analysis. *PLoS ONE*, 3(11):1–7, 2008. ISSN 19326203. doi: 10.1371/journal.pone.0003708.

[21] B Biswal, F Z Yetkin, V M Haughton, and J S Hyde. Functional connectivity in the motor cortex of resting human brain using echo-planar MRI. *Magnetic resonance in medicine : official journal of the Society of Magnetic Resonance in Medicine / Society of Magnetic Resonance in Medicine*, 34(4):537–541, 1995. ISSN 0740-3194. doi: 10.1002/mrm.1910340409.

[22] Linda J. Larson-Prior, Jonathan D. Power, Justin L. Vincent, Tracy S. Nolan, Rebecca S. Coalson, John Zempel, Abraham Z. Snyder, Bradley L. Schlaggar, Marcus E. Raichle, and Steven E. Petersen. Modulation of the brain's functional network architecture in the transition from wake to sleep. *Progress in Brain Research*, 193:277–294, 2011. ISSN 00796123. doi: 10.1016/B978-0-444-53839-0.00018-1.

[23] K. N Bhanu Prakash and Wieslaw L. Nowinski. Morphologic relationship among the corpus callosum, fornix, anterior commissure, and posterior commissure: MRI-based variability study. *Academic Radiology*, 13(1):24–35, 2006. ISSN 10766332. doi: 10.1016/j.acra.2005.06.018.

[24] Lynn K. Paul. Developmental malformation of the corpus callosum: A review of typical callosal development and examples of developmental disorders with

callosal involvement. *Journal of Neurodevelopmental Disorders*, 3(1):3–27, 2011. ISSN 18661947. doi: 10.1007/s11689-010-9059-y.

[25] Bogen JE. The callosal syndromes. *Clinical neuropsychology*, 1979.

[26] *The Parallel Brain: The Cognitive Neuroscience of the Corpus Callosum (Issues in Clinical and Cognitive Neuropsychology)*. MIT, 2002.

[27] Fernanda Tovar-Moll, Jorge Moll, Ricardo De Oliveira-Souza, Ivanei Bramati, Pedro a. Andreiuolo, and Roberto Lent. Neuroplasticity in human callosal dysgenesis: A diffusion tensor imaging study. *Cerebral Cortex*, 17(3):531–541, 2007. ISSN 10473211. doi: 10.1093/cercor/bhj178.

[28] Francisco Aboitiz, Javier López, and Juan Montiel. Long distance communication in the human brain: Timing constraints for inter-hemispheric synchrony and the origin of brain lateralization. *Biological Research*, 36(1):89–99, 2003. ISSN 07169760. doi: 10.4067/S0716-97602003000100007.

[29] Sabine Hofer and Jens Frahm. Topography of the human corpus callosum revisited-Comprehensive fiber tractography using diffusion tensor magnetic resonance imaging. *NeuroImage*, 32(3):989–994, 2006. ISSN 10538119. doi: 10.1016/j.neuroimage.2006.05.044.

[30] M. CHRISTINE PH.D. DE LACOSTE. Topography of the human corpus callosum. *Journal of Neuropathology and Experimental Neurology*, 1985.

[31] Mathias Wahl, Birgit Lauterbach-Soon, Elke Hattingen, Patrick Jung, Oliver Singer, Steffen Volz, Johannes C Klein, Helmuth Steinmetz, and Ulf Ziemann. Human motor corpus callosum: topography, somatotopy, and link between microstructure and function. *The Journal of neuroscience : the official journal of the Society for Neuroscience*, 27(45):12132–12138, 2007. ISSN 0270-6474. doi: 10.1523/JNEUROSCI.2320-07.2007.

[32] David E Stark, Daniel S Margulies, Zarrar E Shehzad, Philip Reiss, a M Clare Kelly, Lucina Q Uddin, Dylan G Gee, Amy K Roy, Marie T Banich, F Xavier Castellanos, and Michael P Milham. Regional variation in interhemispheric coordination of intrinsic hemodynamic fluctuations. *The Journal of neuroscience : the official journal of the Society for Neuroscience*, 28(51):13754–13764, 2008. ISSN 0270-6474. doi: 10.1523/JNEUROSCI.4544-08.2008.

[33] a. Fitsiori, D. Nguyen, a. Karentzos, J. Delavelle, and M. I. Vargas. The corpus callosum: White matter or terra incognita. *British Journal of Radiology*, 84(997):5–18, 2011. ISSN 00071285. doi: 10.1259/bjr/21946513.

[34] Aamish Z Kazi, Priscilla C Joshi, Abhimanyu B Kelkar, Mangal S Mahajan, and Amit S Ghawate. MRI evaluation of pathologies affecting the corpus callosum: A pictorial essay. *The Indian journal of radiology & imaging*, 23(4):321–32, 2013. ISSN 0971-3026. doi: 10.4103/0971-3026.125604. URL http://www.pubmedcentral.nih.gov/articlerender.fcgi?artid=3932574&tool=pmcentrez&rendertype=abstract.

[35] Fernanda Tovar-Moll, Myriam Monteiro, Juliana Andrade, Ivanei E. Bramati, Rodrigo Vianna-Barbosa, Theo Marins, Erika Rodrigues, Natalia Dantas, Timothy E. J. Behrens, Ricardo de Oliveira-Souza, Jorge Moll, and Roberto Lent. Structural and functional brain rewiring clarifies preserved interhemispheric transfer in humans born without the corpus callosum. *Pnas*, 111(21):1400806111–, 2014. ISSN 1091-6490. doi: 10.1073/pnas.1400806111. URL http://www.pnas.org/content/early/2014/05/08/1400806111.

[36] Julia P Owen, Yi-Ou Li, Fanpei G Yang, Charvi Shetty, Polina Bukshpun, Shivani Vora, Mari Wakahiro, Leighton B N Hinkley, Srikantan S Nagarajan, Elliott H Sherr, and Pratik Mukherjee. Resting-state networks and the functional connectome of the human brain in agenesis of the corpus callosum. *Brain connectivity*, 3(6):547–62, 2013. ISSN 2158-0022. doi: 10.1089/brain.2013.0175. URL http://www.pubmedcentral.nih.gov/articlerender.fcgi?artid=3868398&tool=pmcentrez&rendertype=abstract.

[37] Jill X O'Reilly, Paula L Croxson, Saad Jbabdi, Jerome Sallet, Maryann P Noonan, Rogier B Mars, Philip G F Browning, Charles R E Wilson, Anna S Mitchell, Karla L Miller, Matthew F S Rushworth, and Mark G Baxter. Causal effect of disconnection lesions on interhemispheric functional connectivity in rhesus monkeys. *Proceedings of the National Academy of Sciences of the United States of America*, 110(34):13982–7, 2013. ISSN 1091-6490. doi: 10.1073/pnas.1305062110. URL http://www.pubmedcentral.nih.gov/articlerender.fcgi?artid=3752223&tool=pmcentrez&rendertype=abstract.

[38] Steven W. Hetts, Elliott H. Sherr, Stephanie Chao, Sarah Gobuty, and a. James Barkovich. Anomalies of the corpus callosum: An MR analysis of the phenotypic spectrum of associated malformations. *American Journal of Roentgenology*, 187(5):1343–1348, 2006. ISSN 0361803X. doi: 10.2214/AJR.05.0146.

[39] Joana Cabral, Henry Luckhoo, Mark Woolrich, Morten Joensson, Hamid Mohseni, Adam Baker, Morten L. Kringelbach, and Gustavo Deco. Exploring mechanisms of spontaneous functional connectivity in MEG: How delayed network interactions lead to structured amplitude envelopes of band-pass filtered oscillations. *NeuroImage*, 90:423–435, 2014. ISSN 10538119. doi: 10.1016/j.neuroimage.2013.11.047. URL http://dx.doi.org/10.1016/j.neuroimage.2013.11.047.

[40] Marlene Bartos, Imre Vida, and Peter Jonas. Synaptic mechanisms of synchronized gamma oscillations in inhibitory interneuron networks. *Nature reviews. Neuroscience*, 8(1):45–56, 2007. ISSN 1471-003X. doi: 10.1038/nrn2044.

[41] Nicolas Brunel and Xiao-Jing Wang. What determines the frequency of fast network oscillations with irregular neural discharges? I. Synaptic dynamics and excitation-inhibition balance. *Journal of neurophysiology*, 90(1):415–430, 2003. ISSN 0022-3077. doi: 10.1152/jn.01095.2002.

[42] Christoph Börgers and Nancy Kopell. Synchronization in networks of excitatory and inhibitory neurons with sparse, random connectivity. *Neural computation*, 15(3):509–538, 2003. ISSN 0899-7667. doi: 10.1162/089976603321192059.

[43] Patric Hagmann, Maciej Kurant, Xavier Gigandet, Patrick Thiran, Van J. Wedeen, Reto Meuli, and Jean Philippe Thiran. Mapping human whole-brain structural networks with diffusion MRI. *PLoS ONE*, 2(7), 2007. ISSN 19326203. doi: 10.1371/journal.pone.0000597.

[44] Joana R B Cabral. Brain activity during rest. (May), 2012.

[45] Karl Friston. Dynamic Causal Modelling. *Human Brain Function: Second Edition*, 19:1063–1090, 2003. ISSN 10538119. doi: 10.1016/B978-012264841-0/50054-8.

[46] Juan a. Acebrón, L. L. Bonilla, Conrad J Pérez Vicente, Félix Ritort, and Renato Spigler. The Kuramoto model: A simple paradigm for synchronization phenomena. *Reviews of Modern Physics*, 77(1):137–185, 2005. ISSN 00346861. doi: 10.1103/RevModPhys.77.137.

[47] Oleksandr V. Popovych, Yuri L. Maistrenko, and Peter a. Tass. Phase chaos in coupled oscillators. *Physical Review E - Statistical, Nonlinear, and Soft Matter Physics*, 71(6):3–6, 2005. ISSN 15393755. doi: 10.1103/PhysRevE.71.065201.

[48] Wai Shing Lee, Edward Ott, and Thomas M. Antonsen. Large coupled oscillator systems with heterogeneous interaction delays. *Physical Review Letters*, 103(4):4–7, 2009. ISSN 00319007. doi: 10.1103/PhysRevLett.103.044101.

[49] Joana Cabral, Etienne Hugues, Morten L. Kringelbach, and Gustavo Deco. Modeling the outcome of structural disconnection on resting-state functional connectivity. *NeuroImage*, 62(3):1342–1353, 2012. ISSN 10538119. doi: 10.1016/j.neuroimage.2012.06.007. URL http://dx.doi.org/10.1016/j.neuroimage.2012.06.007.

[50] N Tzourio-Mazoyer, B Landeau, D Papathanassiou, F Crivello, O Etard, N Delcroix, B Mazoyer, and M Joliot. Automated anatomical labeling of activations in SPM using a macroscopic anatomical parcellation of the MNI MRI single-subject brain. *NeuroImage*, 15(1):273–289, 2002. ISSN 1053-8119. doi: 10.1006/nimg.2001.0978.

[51] K J Friston, a Mechelli, R Turner, and C J Price. Nonlinear responses in fMRI: the Balloon model, Volterra kernels, and other hemodynamics. *NeuroImage*, 12(4):466–477, 2000. ISSN 1053-8119. doi: 10.1006/nimg.2000.0630.